AD-A097 431 AERONAUTICAL RESEARCH ASSOCIATES OF PRINCETON INC NJ F/G 20/4
FUNDAMENTAL RESEARCH IN TURBULENT MODELING, PART 1, THEORY, PAR--ETC(U)
FEB 81 G SANDRI, C CERASOLI F44620-76-C-0048
UNCLASSIFIED ARAP-438 AFOSR-TR-81-0332 NL

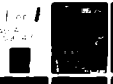

END
DATE FILMED
5-81
DTIC

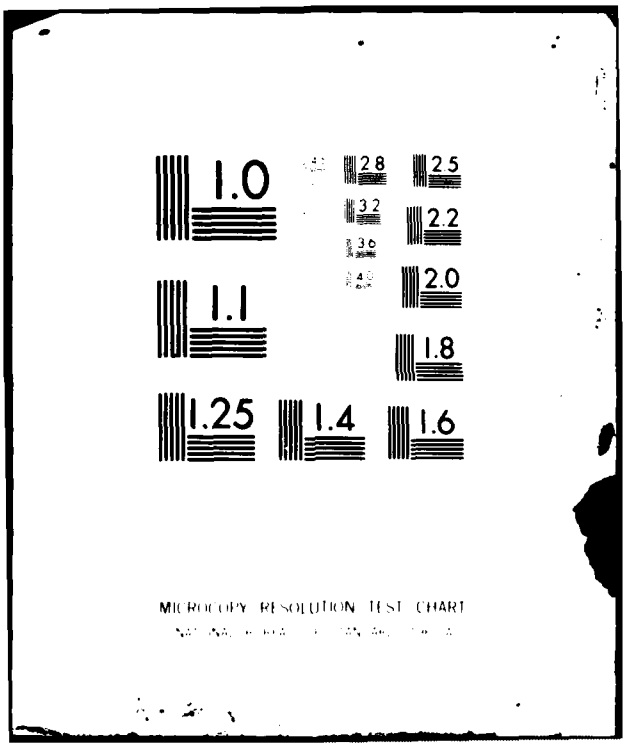
1.0
2.8
2.5
3.2
2.2
3.6
2.0
4.0
1.1
1.8
1.25
1.4
1.6
MICROCOPY RESOLUTION TEST CHART

Unclassified

SECURITY CLASSIFICATION OF THIS PAGE (When Data Entered)

12 87

19 REPORT DOCUMENTATION PAGE

READ INSTRUCTIONS BEFORE COMPLETING FORM

1. REPORT NUMBER	2. GOVT ACCESSION NO.	3. RECIPIENT'S CATALOG NUMBER
18 AFOSR-TR-81-0332	AD-A097431	

4. TITLE (and Subtitle)	5. TYPE OF REPORT & PERIOD COVERED
6 Fundamental Research in Turbulent Modeling, Part 1. Theory. Part 2. Experiment,	9 Final technical rept. 1 JAN 79 — 31 DEC 80
	6. PERFORMING ORG. REPORT NUMBER 438

7. AUTHOR(s)	8. CONTRACT OR GRANT NUMBER(s)
10 Guido Sandri Carmen Cerasoli	15 F44620-76-C-0048

9. PERFORMING ORGANIZATION NAME AND ADDRESS	10. PROGRAM ELEMENT, PROJECT, TASK AREA & WORK UNIT NUMBERS
Aeronautical Research Associates of Princeton, Inc. 50 Washington Road, P.O. Box 2229 Princeton, NJ 08540	2307A2 61102F

11. CONTROLLING OFFICE NAME AND ADDRESS	12. REPORT DATE
Air Force Office of Scientific Research/NA Bldg. 410 Bolling Air Force Base, DC 20332	11 FEB 81
	13. NUMBER OF PAGES 94

14. MONITORING AGENCY NAME & ADDRESS (if different from Controlling Office)	15. SECURITY CLASS. (of this report)
16 2307 17 A2	Unclassified
	15a. DECLASSIFICATION DOWNGRADING SCHEDULE

16. DISTRIBUTION STATEMENT (of this Report)

Approved for public release; distribution unlimited

14 ARAP-438

17. DISTRIBUTION STATEMENT (of the abstract entered in Block 20, if different from Report)

18. SUPPLEMENTARY NOTES

19. KEY WORDS (Continue on reverse side if necessary and identify by block number)

TURBULENCE
SHEAR FLOW
SECOND ORDER CLOSURE
TURBULENCE MODELS
HOMOGENEOUS TURBULENCE

20. ABSTRACT (Continue on reverse side if necessary and identify by block number)

Part 1. Theory

We develop a model of turbulent flows deduced from simple assumptions on the two-point tensor R_{ij} whose first approximation consists in coupled equations for the Reynolds and scale tensors. The model, when specialized to homogeneous turbulence, contains two adjustable parameters with which we match the main features of both grid and sheared turbulence. The calculated integral scales for sheared turbulence are strongly directional. Thus the model allows

DD FORM 1 JAN 73 1473 EDITION OF 1 NOV 65 IS OBSOLETE

Unclassified

SECURITY CLASSIFICATION OF THIS PAGE (When Data Entered)

008400

one to compute, for the first time, a first approximation to the eddy structure in a sheared turbulent flow.

Part 2. Experiment

Data on the mean and fluctuating velocity fields are presented for flow in a pipe with a central rod where the ratio of inner rod diameter to outer pipe diameter was .118. The measurements were taken at a downstream distance of 30 diameters and the turbulent intensities for the three fluctuating velocity components were obtained as a function of radius along with the Reynolds stress. Turbulent length scales were measured by use of time autocorrelation functions in conjunction with Taylor's hypothesis and by two-point correlation measurements using pure radial separations. The present results regarding the flow fields and length scales are compared with previous experimental results and our theoretical knowledge of such flows.

(12

PREFACE

The present report is the final technical report for The Air Force Office of Scientific Research Contract F44620-76-C-0048. The report consists of two parts: Part 1, Theory, by G. Sandri; and Part 2, Experiment, by C. Cerasoli and G. Sandri. The authors acknowledge with pleasure the fundamental contributions of Dr. C. duP. Donaldson to the research effort. They also acknowledge many useful discussions with S. Lewellen, P. Mansfield, R. Sullivan, and J. Yates.

A.R.A.P. Report 438

FUNDAMENTAL RESEARCH IN TURBULENT MODELING

PART 1. THEORY

by

Guido Sandri

TABLE OF CONTENTS

Part 1. Theory

I. INTRODUCTION

The determination of the two-point velocity correlation tensor R_{ij} is a major aim of our research because R_{ij} contains full information on the Reynolds stress tensor, the scale and the structure of an arbitrary turbulent flow. The tensor R_{ij} is defined by

$$R_{ij}(\vec{x},\vec{y}) = \left\langle u_i'(\vec{x})u_j'(\vec{y})\right\rangle$$

We propose to determine R_{ij} by solving a closed equation for this quantity (Refs. 1, 2). Closure requires modeling of the nonlinear velocity correlation terms analogous to those now familiar in second-order closures for the Reynolds stresses (Ref. 3). Because R_{ij} contains scale and structure information, closure of the R_{ij} equation obviates the need for introducing *ad hoc* information on these features of the turbulence.

As a first attack on the integration of the modeled R_{ij} equations for a general flow, we simplify the integration by introducing the approximation

$$R_{ij} = \frac{q^2}{3}\Lambda_{ij}\delta(|\vec{r}|) \tag{1}$$

which is the first term in the moment expansion of R_{ij} in the relative coordinate $\vec{r} = \vec{x} - \vec{y}$. Here Λ_{ij} is the angular or Batchelor average of the integral scale for the appropriate component of the two-point correlation tensor; i.e.,

$$\frac{q^2}{3}\Lambda_{ij} = \int \frac{R_{ij}}{4\pi r^2}\, d\vec{r} \tag{2}$$

This "first moment" approximation yields coupled equations for the Reynolds stress and for the scale tensor. Since both quantities are single-point variables, the approximation is relatively simple when compared to the full system, which is a two-point, multicomponent equation.

We note that for isotropic turbulence, as discussed in Ref. 1, we have, with $\Lambda = \Lambda_{kk}/3$

1. Sandri, G., "A New Approach to the Development of Scale Equations for Turbulent Flows," A.R.A.P. Report No. 302, April 1977.
2. Sandri, G., "Recent Results Obtained in the Modeling of Turbulent Flows by Second-Order Closure," AFOSR-TR-78-0680, February 1978.
3. Donaldson, C.duP., "Construction of a Dynamic Model of the Production of Atmospheric Turbulence and the Dispersal of Atmospheric Pollutants," Workshop on Micrometeorology (D.A. Haugen, ed.), American Meteorological Society, Boston (1973), pp. 313-392.

$$\frac{3}{2}\Lambda = \frac{1}{2}\Lambda_{kk} = L_f = \int_0^\infty f(r)\, dr \qquad (3)$$

where $r = |\vec{r}|$. Since L_f is G.I. Taylor's integral scale, Eq. (3) justifies our statement that the tensor Λ_{ij} represents an integral scale.

The first moment approximation is based on the assumption that the size of the eddies is small compared to the scale of the mean quantities. This assumption is not usually valid, so that for a number of flows we must consider the full R_{ij} equation. Fortunately, however, we can test the first moment approximation quite stringently. In fact, (i) the first moment approximation is valid for homogeneous flows, whether sheared or not, because for such flows the scale of the mean is infinite, and (ii) several experiments have been performed on homogeneous flows, with and without shear, which yield information on several turbulence quantities.

Our model, which contains only two adjustable parameters, is required to reproduce the main features of both grid and sheared turbulence data. We find a satisfactory overall fit with parameter choices that are used in second-order closure for general flows. The calculated integral scales for sheared turbulence are strongly directional. Thus the model allows one to compute, for the first time, a first approximation of the eddy structure in a sheared turbulent flow.

Proceeding a step beyong the first moment approximation, we show that the familiar dissipation equation

$$\frac{\partial q^2}{\partial t} = -2b\,\frac{q^3}{\Lambda}$$

can be derived from a simple model of the "cascading" term (the divergence of the triple velocity correlation).

II. DERIVATION OF CLOSED EQUATIONS FOR THE TWO-POINT CORRELATION TENSOR

We start with the Navier-Stokes equations for the velocity field u_i and the kinematic pressure p (pressure/density)

$$\frac{\partial u_i}{\partial t} + u_k \frac{\partial u_i}{\partial x_k} + \frac{\partial p}{\partial x_i} = \nu \nabla^2 u_i \tag{4}$$

$$\frac{\partial u_i}{\partial x_i} = 0 \tag{5}$$

The velocity and pressure are decomposed, following Reynolds, into mean and fluctuating parts

$$u_i = \overline{u_i} + u_i' \tag{6}$$

$$p = \bar{p} + p' \tag{7}$$

Substituting (6) and (7) into (4) and (5), one obtains separate equations for the mean and fluctuations. After multiplication and averaging, these equations can be cast into the form of equations for the correlation tensor R_{ij}

$$R_{ij}(\vec{x},\vec{y}) = \left\langle u_i'(\vec{x}) u_j'(\vec{y}) \right\rangle \tag{8}$$

namely,

$$\begin{aligned}
\frac{\partial R_{ij}}{\partial t} = &- \left[\bar{u}_k(\vec{x}) \frac{\partial}{\partial x_k} + \bar{u}_k(\vec{y}) \frac{\partial}{\partial y_k} \right] R_{ij} + \\
&- \left[R_{ik} \frac{\partial \bar{u}_j}{\partial y_k} + \frac{\partial \bar{u}_i}{\partial x_k} R_{kj} \right] + \\
&- \left[\frac{\partial}{\partial x_k} \left\langle u_i'(\vec{x}) u_k'(\vec{x}) u_j'(\vec{y}) \right\rangle + \frac{\partial}{\partial y_k} \left\langle u_i'(\vec{x}) u_k'(\vec{y}) u_j'(\vec{y}) \right\rangle \right] + \\
&- \left[\left\langle \frac{\partial p'}{\partial x_i} u_j'(\vec{y}) \right\rangle + \left\langle u_i'(\vec{x}) \frac{\partial p'}{\partial y_j} \right\rangle \right] + \nu \left[\left(\nabla_x^2 + \nabla_y^2 \right) R_{ij} \right]
\end{aligned} \tag{9}$$

and

$$\frac{\partial R_{ij}}{\partial x_i} = 0 \tag{10}$$

$$\frac{\partial R_{ij}}{\partial y_j} = 0 \tag{11}$$

It is convenient to recast these equations by introducing "centroid" and "relative" variables as follows:

$$\vec{x}_c = \frac{\vec{x} + \vec{y}}{2} \tag{12}$$

$$\vec{r} = \vec{y} - \vec{x} \tag{13}$$

Using the chain rule for differentiation, as detailed in Ref. 1, the dynamical equations for R_{ij} become

$$\begin{aligned}
\frac{\partial R_{ij}}{\partial t} = &-\left[\frac{\bar{u}_k(\vec{x}) + \bar{u}_k(\vec{y})}{2} \frac{\partial}{\partial x_{ck}} + \left(\bar{u}_k(\vec{y}) - \bar{u}_k(\vec{x})\right) \frac{\partial}{\partial r_k} \right] R_{ij} + \\
&-\left[R_{ik} \frac{\partial \bar{u}_j}{\partial x_{ck}} + \frac{\partial \bar{u}_i}{\partial x_{ck}} R_{kj} \right] + \\
&- \frac{1}{2} \frac{\partial}{\partial x_{ck}} \left[\left\langle u_i'(\vec{x}) u_k'(\vec{x}) u_j'(\vec{y}) \right\rangle + \left\langle u_i'(\vec{x}) u_k'(\vec{y}) u_j'(\vec{y}) \right\rangle \right] + \\
&+ \frac{\partial}{\partial r_k} \left[\left\langle u_i'(\vec{x}) u_k'(\vec{x}) u_j'(\vec{y}) \right\rangle - \left\langle u_i'(\vec{x}) u_k'(\vec{y}) u_j'(\vec{y}) \right\rangle \right] + \\
&-\left[\frac{\partial}{\partial x_{ci}} \left\langle p'(\vec{x}) u_j'(\vec{y}) \right\rangle + \frac{\partial}{\partial x_{cj}} \left\langle u_i'(\vec{x}) p'(\vec{y}) \right\rangle \right] + \\
&+\left[\left\langle p'(\vec{x}) \frac{\partial u_j'(\vec{y})}{\partial x_{ci}} \right\rangle + \left\langle \frac{\partial u_i'(\vec{x})}{\partial x_{cj}} p'(\vec{y}) \right\rangle \right] + \\
&+ \nu \nabla_c^2 R_{ij} - 2\nu \left\langle \frac{\partial u_i'(\vec{x})}{\partial x_{ck}} \frac{\partial u_j'(\vec{y})}{\partial x_{ck}} \right\rangle
\end{aligned} \tag{14}$$

and the continuity equations become

$$\frac{\partial R_{ij}}{\partial x_{ci}} = 2 \frac{\partial R_{ij}}{\partial r_i} \tag{15}$$

$$\frac{\partial R_{ij}}{\partial x_{cj}} = -2 \frac{\partial R_{ij}}{\partial r_j} \tag{16}$$

where the arguments in the correlations are given by the inverse of Eqs. (12) and (13), namely,

$$\vec{x} = \vec{x}_c - \frac{\vec{r}}{2} \tag{17}$$

$$\vec{y} = \vec{x}_c + \frac{\vec{r}}{2} \tag{18}$$

For homogeneous turbulence, the derivatives with respect to the centroid vanish when acting on any correlation but not, in general, on the mean velocity or on a fluctuation. We then have, for homogeneous turbulence, the dynamical equations

$$\begin{aligned}\frac{\partial R_{ij}}{\partial t} = &-\left[\bar{u}_k(\vec{y}) - \bar{u}_k(\vec{x})\right] \frac{\partial R_{ij}}{\partial r_k} - \left[R_{ik} \frac{\partial \bar{u}_j}{\partial x_{ck}} + \frac{\partial \bar{u}_i}{\partial x_{ck}} R_{kj}\right] + \\ &+ \frac{\partial}{\partial r_k}\left[\left\langle u_i'(\vec{x}) u_k'(\vec{x}) u_j'(\vec{y})\right\rangle - \left\langle u_i'(\vec{x}) u_k'(\vec{y}) u_j'(\vec{y})\right\rangle\right] + \\ &+ \left[\left\langle p'(\vec{x}) \frac{\partial u_j'(\vec{y})}{\partial x_{ci}}\right\rangle + \left\langle \frac{\partial u_i'(\vec{x})}{\partial x_{cj}} p'(\vec{y})\right\rangle\right] + \\ &- 2\nu \left\langle \frac{\partial u_i'(\vec{x})}{\partial x_{ck}} \frac{\partial u_j'(\vec{y})}{\partial x_{ck}}\right\rangle\end{aligned} \tag{19}$$

and the continuity conditions

$$\frac{\partial R_{ij}}{\partial r_i} = 0 \tag{20}$$

$$\frac{\partial R_{ij}}{\partial r_j} = 0 \tag{21}$$

The terms in Eq. (19) that prevent closure of the equation are the last three. In order to achieve closure, we introduce generalized transport models as follows:

(i) Dissipation equation. We shall prove in Section V that a model for dissipation is not needed once a model for eddy size rearrangement is specified. A full specification of this latter is not available at present; therefore, we provisionally maintain a model for dissipation which is given by

$$-2\nu \left\langle \frac{\partial u_i'(\vec{x})}{\partial x_{ck}} \frac{\partial u_j'(\vec{y})}{\partial x_{ck}} \right\rangle = -2\left(\frac{bq}{\Lambda}\right) \frac{\delta_{ij}}{3} R_{\alpha\alpha}(\vec{r}) \tag{22}$$

(ii) Intercomponent rearrangement. We give a generalization of the familiar tendency-towards-isotropy model by introducing a tensor C_{ij} that guarantees that continuity is satisfied.

$$\left\langle p'(\vec{x}) \frac{\partial u_j'(\vec{y})}{\partial x_{ci}} + \frac{\partial u_i'(\vec{x})}{\partial x_{cj}} p'(\vec{y}) \right\rangle = -\frac{q}{\Lambda}\left[R_{ij} - \frac{1}{3}\delta_{ij}R_{\alpha\alpha} + C_{ij}\right] \tag{23}$$

The tensor C_{ij} is assumed to satisfy

$$C_{ij}(\vec{r} = 0) = 0 \tag{24}$$

$$\int \frac{C_{ij}(\vec{r})}{4\pi r^2} d\vec{r} \tag{25}$$

These properties are utilized in Section III to derive the Reynolds stress and scale tensor equations. In the Appendix, we prove a rather remarkable property of C_{ij} for isotropic turbulence. If S_{ij} satisfies continuity (as we assume here), the tensor C_{ij} is uniquely determined by continuity and it is such as to make the pressure-velocity correlations vanish as is necessary for isotropic turbulence. A proof of the latter statement is given in Ref. 4, p. 51.

(iii) Eddy size rearrangement. In addition to the two generalizations given above, we need a model for the spatially homogeneous part of the triple velocity correlation which represents the nonlinear effects of local turbulent convection. These nonlinear effects correspond to either eddy break-up (cascading, when wave vectors add) or merging of eddies (when the wave vectors subtract). We assume the model

$$\frac{\partial}{\partial r_k}\left[\left\langle u_i'(\vec{x})u_k'(\vec{x})u_j'(\vec{y})\right\rangle - \left\langle u_i'(\vec{x})u_k'(\vec{y})u_j'(\vec{y})\right\rangle\right] = v'\frac{q}{\Lambda}\left[R_{ij} - S_{ij}\right] \tag{26}$$

---

4. Batchelor, G.K., The Theory of Homogeneous Turbulence, Cambridge University Press, 1953.

where S_{ij} satisfies

$$S_{ij}(\vec{r} = 0) = \overline{u_i' u_j'} \tag{27}$$

$$\int \frac{S_{ij}}{4\pi r^2} d\vec{r} = 0 \tag{28}$$

A simple example of N_{ij} is

$$S_{ij} = \frac{\partial^n}{\partial |r|^n} \left(|r|^n R_{ij} \right)$$

where n is a positive integer. Substituting the models (22), (23) and (26) into (19) yields

$$\frac{\partial R_{ij}}{\partial t} = - \left[\bar{u}_k(\vec{y}) - \bar{u}_k(\vec{x}) \right] \frac{\partial R_{ij}}{\partial r_k} - \left[R_{ik} \frac{\partial \bar{u}_j}{\partial x_{ck}} + \frac{\partial \bar{u}_i}{\partial x_{ck}} R_{kj} \right] +$$

$$+ v' \frac{q}{\Lambda} \left[R_{ij} - S_{ij} \right] - \frac{q}{\Lambda} \left[R_{ij} - \frac{1}{3} \delta_{ij} R_{\alpha\alpha} + C_{ij} \right] +$$

$$- 2 \left(\frac{bq}{\Lambda} \right) \frac{\delta_{ij}}{3} R_{\alpha\alpha} \tag{29}$$

with (20) and (21), i.e., continuity, holding.

We also introduce the spectral tensor ϕ_{ij} in order to present the equations in separation space as well as wave number space. The definition is

$$\phi_{ij}(\vec{k}) = \frac{1}{(2\pi)^3} \int R_{ij}(\vec{r}) \, e^{i\vec{k} \cdot \vec{r}} \, d\vec{r}$$

The unmodeled equation for the spectral tensor ϕ_{ij} is

$$\frac{\partial \phi_{ij}}{\partial t} - U' k_1 \frac{\partial}{\partial k_2} \phi_{ij} =$$

$$= - U' (\phi_{i2} \delta_{j1} + \delta_{2i} \phi_{2j}) - i \left[\Phi_{ij}(\vec{k}) + \Phi_{ji}(-\vec{k}) \right]$$

$$+ i \left[k_i P_j(\vec{k}) - k_j P_i(-\vec{k}) \right] - 2\nu k^2 \phi_{ij}$$

where we have introduced the two spectra

$$\Phi_{ij}(\vec{k}) = k_\alpha \int T_{i\alpha j}(\vec{r}) \, e^{-i\vec{k}\cdot\vec{r}} \, \frac{d\vec{r}}{(2\pi)^3}$$

$$P_j(\vec{k}) = \int \left\langle p'(\vec{x}) u_j'(\vec{y}) \right\rangle e^{-i\vec{k}\cdot\vec{r}} \, \frac{d\vec{r}}{(2\pi)^3}$$

and the triple velocity correlation tensor

$$T_{i\alpha j}(\vec{r}) = \left\langle u_i(\vec{x}) u_\alpha(\vec{x}) u_j(\vec{x} + \vec{r}) \right\rangle$$

Continuity requires the Poisson equation

$$ik^2 \frac{P_j(\vec{k}) - P_j(-\vec{k})}{2} = 2U' k_1 \phi_{2j} + ik_\alpha \left[\Phi_{\alpha j}(\vec{k}) + \Phi_{\alpha j}(-\vec{k}) \right]$$

Anticipating the development of Section V, we note that the following simple model gives a tolerable picture for the energy spectrum of grid turbulence

$$-i \left[\Phi_{ij}(\vec{k}) + \Phi_{ji}(-\vec{k}) \right] =$$

$$= \frac{q}{\Lambda} \left[A\phi_{ij} + B \; k \frac{\partial}{\partial k} \phi_{ij} + 2\phi_{ij} \; + C \left(k^2 \frac{\partial^2}{\partial k^2} \phi_{ij} + 4k \frac{\partial}{\partial k} \phi_{ij} + 2\phi_{ij} \right) \right]$$

with

$$A \approx 0.075 \; , \quad B \approx 0.615 \; , \quad C \approx 0.27$$

which have been adjusted to give exactly a 5/3 law for equilibrium.

A full matching of the energy spectrum as a function of time is not achieved with this model; mainly the peak value is followed correctly. We attribute this feature in part to the fact that a grid flow is not simply an isotropic flow. In Section V we discuss a simpler form of the model to demonstrate an important relation between dissipation and eddy size rearrangement.

III. EQUATIONS FOR THE REYNOLDS AND SCALE TENSORS

We now exploit the definition

$$\overline{u_i' u_j'} = \lim_{\vec{r} \to 0} R_{ij}(\vec{r})$$

in order to obtain the rate equation for the Reynolds stress (divided by ρ). We let $\vec{r} \to 0$ in (29) and find, using (24) and (27)

$$\frac{\partial}{\partial t} \overline{u_i' u_j'} = -\left[\overline{u_i' u_k'} \frac{\partial \bar{u}_j}{\partial x_{ck}} + \frac{\partial \bar{u}_i}{\partial x_{ck}} \overline{u_k' u_j'} \right] - \frac{q}{\Lambda}\left[\overline{u_i' u_j'} - \frac{1}{3} \delta_{ij} q^2 \right]$$

$$- 2\left(\frac{bq}{\Lambda}\right) \frac{1}{3} \delta_{ij} q^2 \qquad (30)$$

The scale tensor, Λ_{ij}, is defined in terms of R_{ij} by

$$\frac{q^2}{3} \Lambda_{ij} \equiv \int \frac{R_{ij}}{4\pi r^2} \, d\vec{r} \qquad (31)$$

To obtain a rate equation for the scale tensor Λ_{ij} that includes the first order information of turbulence structure, we expand $R_{ij}(\vec{r})$ in terms of its moments in pure relative coordinates and retain the lowest term. We obtain

$$R_{ij}(r) = \frac{q^2}{3} \Lambda_{ij} \delta(|\vec{r}|) \qquad (32)$$

where the Dirac function of the magnitude of $\vec{r}$ is related to $\delta(\vec{r})$ by

$$\delta(\vec{r}) = \frac{\delta(|\vec{r}|)}{4\pi r^2} \qquad (33)$$

We use the notation $r = |\vec{r}|$. The approximation (33), as we remarked in the Introduction, is best justified for homogeneous turbulence because in this case the spatial scale of the mean flow is infinite.

We now apply to (29) the operation $\int d\vec{r}/4\pi r^2$ and, using (25) and (28), we find

$$\frac{\partial}{\partial t}\left(q^2\Lambda_{ij}\right) = -q^2\left[\Lambda_{ik}\frac{\partial \bar{u}_j}{\partial x_{ck}} + \frac{\partial \bar{u}_i}{\partial x_{ck}}\Lambda_{kj}\right] + \left(v' \frac{q}{\Lambda}\right)q^2\Lambda_{ij} +$$

$$- \frac{q}{\Lambda}\left[q^2\Lambda_{ij} - \frac{1}{3}\delta_{ij}q^2\Lambda_{kk}\right] - 2bq^3\delta_{ij} \qquad (34)$$

Convection of Λ_{ij} does not occur for homogeneous turbulence. To see that this fact is a consequence of the moment approximation (32), we note that (33) gives

$$\int \frac{d\vec{r}}{4\pi r^2}\left[\bar{u}_k\left(\vec{x}_c + \frac{\vec{r}}{2}\right) - \bar{u}_k\left(\vec{x}_c - \frac{\vec{r}}{2}\right)\right]\frac{\partial}{\partial r_k}\delta(|\vec{r}|)$$

$$= \int \frac{d\vec{r}}{4\pi r^2}\left[\bar{u}_k\left(\vec{x}_c + \frac{\vec{r}}{2}\right) - \bar{u}_k\left(\vec{x}_c - \frac{\vec{r}}{2}\right)\right]\frac{\partial}{\partial r_k}\left(4\pi r^2\delta(\vec{r})\right)$$

$$= -\int d\vec{r}\,\delta(\vec{r})\left[\frac{\partial}{\partial x_{ck}}\bar{u}_k\left(\vec{x}_c + \frac{\vec{r}}{2}\right) + \frac{\partial}{\partial x_{ck}}\bar{u}_k\left(\vec{x}_c - \frac{\vec{r}}{2}\right)\right]$$

$$= -2\frac{\partial \bar{u}_k(\vec{x}_c)}{\partial x_{ck}} = 0$$

where we performed an integration by parts and used continuity. We obtain the final form of the equation for the scale tensor by substituting into (34) the formula

$$\frac{\partial}{\partial t}\left(q^2\Lambda_{ij}\right) = q^2\frac{\partial \Lambda_{ij}}{\partial t} + \Lambda_{ij}\frac{\partial q^2}{\partial t} \qquad (35)$$

and the contraction of Eq. (30)

$$\frac{\partial q^2}{\partial t} = -2\overline{u_i'u_k'}\frac{\partial \bar{u}_k}{\partial x_{ci}} - 2b\frac{q^3}{\Lambda} \qquad (36)$$

This latter is the energy equation. The result is

$$\frac{\partial \Lambda_{ij}}{\partial t} = -\left[\Lambda_{ik} \frac{\partial \bar{u}_j}{\partial x_{ck}} + \frac{\partial \bar{u}_i}{\partial x_{ck}} \Lambda_{kj} \right] + \Lambda_{ij} \left[2 \frac{\overline{u_k' u_\ell'}}{q^2} \frac{\partial \bar{u}_k}{\partial x_{c\ell}} + \frac{q}{\Lambda} (2b + v') \right] +$$

$$- \frac{q}{\Lambda} \left[\Lambda_{ij} - \frac{\delta_{ij}}{3} \Lambda_{kk} \right] - 2bq\delta_{ij} \qquad (37)$$

Note that Eq. (37) us ibtained by dividing by q^2 and, therefore, it is meaningless in the absence of turbulence.

To close the pair (30) and (37), we choose

$$\Lambda = \frac{1}{3} \Lambda_{kk} \qquad (38)$$

The reason for this choice was discussed in a previous report (Ref. 1). Contraction of (37) and use of (38) yields the equation for the mean scale

$$\frac{\partial \Lambda}{\partial t} = -\frac{2}{3} \Lambda_{ik} \frac{\partial \bar{u}_i}{\partial x_{ck}} + \Lambda \frac{2\overline{u_k' u_\ell'}}{q^2} \frac{\partial \bar{u}_k}{\partial x_{c\ell}} + v'q \qquad (39)$$

It is interesting to note that, in this model, the coefficient of the "production" term is not a universal constant and receives generally competing contributions from the Reynolds stress and from the tensor scale.

IV. SOLUTIONS OF THE COUPLED EQUATIONS FOR STRESS AND SCALE TENSORS

In this section we give two analytic solutions to the coupled equations for the stress tensor and scale tensor equations. We use subsections to separate the different calculations.

A. Equations in Standard Coordinates

The centroid vector and mean velocity vector are taken to have components

$$(x,y,z) \ , \ (U(y),0,0)$$

with $\partial U/\partial y = U' =$ constant. The relevant components of the Reynolds stress equations are obtained from Eqs. (30) and (36). We drop primes on the fluctuations and give a form useful for numerical integration in which $\overline{u_1^2}$ and Λ_{11} are calculated from

$$\overline{u_1^2} = q^2 - \overline{u_2^2} - \overline{u_3^2} \tag{40}$$

$$\Lambda_{11} = 3\Lambda - \Lambda_{22} - \Lambda_{33} \tag{41}$$

The other relevant components of the stress and energy equations are

$$\frac{\partial}{\partial t}\overline{u_2^2} = \frac{1}{3}(1 - 2b)\frac{q^3}{\Lambda} - \frac{q}{\Lambda}\overline{u_2^2} \tag{42}$$

$$\frac{\partial}{\partial t}\overline{u_3^2} = \frac{1}{3}(1 - 2b)\frac{q^2}{\Lambda} - \frac{q}{\Lambda}\overline{u_3^2} \tag{43}$$

$$\frac{\partial}{\partial t}\overline{u_1u_2} = -u_2^2\, U' - \frac{q}{\Lambda}\overline{u_1u_2} \tag{44}$$

$$\frac{\partial q}{\partial t} = -\frac{\overline{u_1u_2}}{q}U' - b\frac{q^2}{\Lambda} \tag{45}$$

For the tensor scale components, we obtain, using Eqs. (37) and (39)

$$\frac{\partial}{\partial t}\Lambda_{22} = -\frac{1}{T}\Lambda_{22} + (1 - 2b)q \tag{46}$$

$$\frac{\partial}{\partial t}\Lambda_{33} = -\frac{1}{T}\Lambda_{33} + (1 - 2b)q \tag{47}$$

$$\frac{\partial}{\partial t}\Lambda_{12} = -\frac{1}{T}\Lambda_{12} - U'\Lambda_{22} \tag{48}$$

$$\frac{\partial}{\partial t}\Lambda = 2\frac{\overline{u_1u_2}}{q^2}U'\Lambda - \frac{2}{3}\Lambda_{12}U' + v'q \tag{49}$$

where

$$\frac{1}{T} = -2\frac{\overline{u_1u_2}}{q^2}U' + \frac{q}{\Lambda}(1 - 2b - v') \tag{50}$$

B. Solution of the Shearless Equations

Setting $U' = 0$, we see that equations for q and Λ decouple from the tensor components. Introducing the deviators

$$d_{ij} = \overline{u_iu_j} - \frac{1}{3}\delta_{ij}q^2 \tag{51}$$

$$D_{ij} = \Lambda_{ij} - \frac{1}{3}\delta_{ij}\Lambda_{kk} \tag{52}$$

and the time

$$\tau = \frac{\Lambda}{q} \tag{53}$$

We have the set

$$\frac{\partial}{\partial t}q = -\frac{b}{\tau}q \quad , \quad \frac{\partial}{\partial t}\Lambda = \frac{v'}{\tau}\Lambda \tag{54}$$

$$\frac{\partial}{\partial t}d_{ij} = -\frac{b}{\tau}d_{ij} \quad , \quad \frac{\partial}{\partial t}D_{ij} = -\frac{1 - 2b - v'}{\tau}D_{ij} \tag{55}$$

$$\frac{\partial}{\partial t}\tau = b + v' \tag{56}$$

Integrating (56) as

$$\tau = (b + v')(t - t_o) + \frac{\Lambda_o}{q_o} \tag{57}$$

we see that q , Λ , d_{ij} and D_{ij} are suitable powers of $(q_o/T_o)\tau$; for example,

$$q = q_o\left[(b + v') \frac{q_o}{\Lambda_o} (t - t_o) + 1\right]^{-b/(b+v')} \tag{58}$$

$$d_{ij} = d_{ij_o}\left[(b + v') \frac{q_o}{\Lambda_o} (t - t_o) + 1\right]^{-1/(b+v')} \tag{59}$$

$$\Lambda = \Lambda_o\left[(b + v') \frac{q_o}{\Lambda_o} (t - t_o) + 1\right]^{-v'/(b+v')} \tag{60}$$

A good fit to experimental data on the decay of turbulent energy and the growth of eddy size for grid turbulence is obtained if one chooses

$$b \simeq \frac{1}{8} \quad , \quad v' \simeq 0.075 \tag{61}$$

We then see that for large times

$$q^2 \sim q_o^2 \left[\cdot 2 \frac{q_o}{\Lambda_o} t \right]^{-5/4} \tag{62}$$

$$d_{ij} \sim d_{ij_o}\left[\cdot 2 \frac{q_o}{\Lambda_o} t \right]^{-5} \tag{63}$$

which shows that the deviator decays with a power about four times larger than the energy. This substantial difference may eventually be checked in our anisotropic grid flow.

From the solutions given above, we can verify that statistics are preserved by the model equations if the model parameters satisfy certain bounds. We first show that the two tensors $\overline{u_iu_j}$ and Λ_{ij} are positive definite from their definitions. Consider an arbitrary (constant) A_i then,

$$A_i\overline{u_iu_j}A_j = \overline{(u\cdot A)^2} \geq 0 \tag{64}$$

the equality sign holding for $A \equiv 0$ only. Thus $\overline{u_iu_j}$ is a positive definite tensor.

From the definition of the scale tensor given by Eq. (31), using Fourier transform on R_{ij} ,

$$\frac{q^2}{3}\Lambda_{ij} = \int \frac{R_{ij}}{4\pi r^2}\, d\vec{r} = \int \frac{\phi_{ij}}{8\pi k}\, d\vec{k} \tag{65}$$

where the power spectrum tensor ϕ_{ij} is positive definite by Khiutchine's theorem. Thus,

$$\frac{q^2}{3} A_i \Lambda_{ij} A_j = \int \frac{d\vec{k}}{8\pi k} A_i \phi_{ij} A_j \geq 0 \tag{66}$$

Thus, Λ_{ij} is positive definite because q^2 is positive as a consequence of (64).

Using the solution (61) and an analogous solution for Λ_{ij}, we find

$$\overline{u_i u_j}(t) = \overline{u_i u_j}(0)\left(\frac{q_o}{\Lambda_o}\tau\right)^{-1/(b+v')} + \frac{1}{3}\delta_{ij} q_o^2 \left[\left(\frac{q_o}{\Lambda_o}\tau\right)^{-2b/(b+v')} - \left(\frac{q_o}{\Lambda_o}\tau\right)^{-1/(b+v')}\right] \tag{67}$$

$$\Lambda_{ij}(t) = \Lambda_{ij}(0)\left(\frac{q_o}{\Lambda_o}\tau\right)^{-(1-2b-v')/(b+v')} + \Lambda(0)\delta_{ij}\left[\left(\frac{q_o}{\Lambda_o}\tau\right)^{v'/(b+v')} - \left(\frac{q_o}{\Lambda_o}\tau\right)^{-(1-2b-v')/(b+v')}\right] \tag{68}$$

We now multiply (67) by $A_i A_j$ when A_i is an arbitrary vector and find

$$A_i \overline{u_i u_j}(t) A_j = \overline{(A\cdot u)^2}(0)\left(\frac{q_o}{\Lambda_o}\tau\right)^{-1/(b+v')} + \frac{A^2}{3} q_o^2 \left[\left(\frac{q_o}{\Lambda_o}\tau\right)^{-2b/(b+v')} - \left(\frac{q_o}{\Lambda_o}\tau\right)^{-1/(b+v')}\right] \tag{69}$$

From (57) we see that

$$\frac{q_o}{\Lambda_o}\tau \geq 1 \qquad (b + v' \geq 0) \tag{70}$$

Sufficient for the left-hand side of (69) to be positive is

$$\left(\frac{q_o}{\Lambda_o}\tau\right)^{-2b/(b+v')} \geq \left(\frac{q_o}{\Lambda_o}\tau\right)^{-1/(b+v')} \tag{71}$$

which requires, using (70),

$$2b \leq 1 \tag{72}$$

A similar analysis applies to Λ_{ij} ; however, no further restrictions on the parameters is found.

C. An Exact Solution of the Equations with Shear

To obtain a solution of the equations with shear, we let

$$\begin{aligned} q &= V\, e^{aU't} & \Lambda &= L\, e^{aU't} \\ \overline{u_1^2} &= W_1\, e^{2aU't} & \Lambda_{11} &= L_1\, e^{aU't} \\ \overline{u_2^2} &= W_2\, e^{2aU't} & \Lambda_{22} &= L_2\, e^{aU't} \\ \overline{u_3^2} &= W_3\, e^{2aU't} & \Lambda_{33} &= L_3\, e^{aU't} \\ \overline{u_1 u_2} &= W_4\, e^{2aU't} & \Lambda_{12} &= L_4\, e^{aU't} \end{aligned} \tag{73}$$

Substituting these forms into the differential equations of III.A, we find that the exponentials cancel and that an algebraic set of equations for the amplitudes are obtained. It is possible, with some algebra, to solve the amplitude equations explicitly in terms of the parameters b and v' . The energy components are

$$\frac{\overline{u_1^2}}{q^2} = \frac{1 + 6v' + 4b}{3(1 + 2v')} \tag{74}$$

$$\frac{\overline{u_2^2}}{q^2} = \frac{u_3^2}{q^2} = \frac{1 - 2b}{3}\,\frac{1}{1 + 2v'} \tag{75}$$

The scale components are

$$\frac{\Lambda_{11}}{\Lambda} = \frac{1 + 6v' + 4b}{1 + 2v'} \tag{76}$$

$$\frac{\Lambda_{22}}{\Lambda} = \frac{\Lambda_{33}}{\Lambda} = \frac{1 - 2b}{1 + 2v'} \tag{77}$$

We see that

$$\frac{\Lambda_{11}}{\Lambda_{22}} = \frac{\overline{u_1^2}}{\overline{u_2^2}} = \frac{1 + 6v' + 4b}{1 - 2b} \tag{78}$$

The off-diagonal components are

$$Br = \frac{|\overline{u_1 u_2}|}{q^2} = \frac{1}{1 + 2v'} \sqrt{\frac{(1 - 2b)(b + v')}{3}} \tag{79}$$

$$\frac{\Lambda_{12}}{\Lambda} = - \frac{1}{1 + 2v'} \sqrt{3(1 - 2b)(b + v')} \tag{80}$$

The Corrsin parameter is

$$C \equiv \frac{\overline{u_1 u_2}}{\sqrt{\overline{u_1^2}\,\overline{u_2^2}}} = \sqrt{\frac{3(b + v')}{1 + 4b + 6v'}} \tag{81}$$

The ratio of the two times is

$$\frac{1}{\alpha} = \frac{q}{U'\Lambda} = \frac{1}{1 + 2v'} \sqrt{\frac{1 - 2b}{3(b + v')}} \tag{82}$$

and the growth rate, a , is

$$a = v' \frac{1}{\alpha} = \frac{v'}{1 + 2v'} \sqrt{\frac{1 - 2b}{3(b + v')}} \tag{83}$$

We notice two additional interesting parameters:

$$\frac{|\overline{u_1 u_2}|}{q^2} \frac{U'}{q} = \alpha \cdot Br = b + v' \tag{84}$$

$$\frac{\Lambda_{ij}}{\Lambda} - \delta_{ij} = 3\left(\frac{\overline{u_i u_j}}{q^2} - \frac{1}{3}\delta_{ij}\right) \tag{85}$$

In terms of the anisotropy parameter σ defined in Ref. 2, p. 4, we note that this condition corresponds exactly to

$$\sigma = 3$$

The value of σ that has given satisfactory results for a wide class of turbulent flows is

$$\sigma_{exp} = 2.5$$

We add the following observations:

1) Several numerical integrations suggest that any solution that is statistically realizable initially will remain so and will asymptote to the exact solutions given.

2) If the scalar scale equation

$$\frac{\partial \Lambda}{\partial t} = c \frac{\Lambda}{2} \overline{u_1 u_2} U' + v'q \qquad (c \approx 0.35) \tag{86}$$

is adopted instead of the tensor equation, an exponential solution exists and has the same qualitative features insofar as scale and energy are concerned (of course, no scale directivity results). This indicates that the models for scale, which were <u>not</u> designed to fit homogeneous shear data, are quite stable.

With only two adjustable constants, the model covers qualitatively both types of turbulent flows. We have shown this by exhibiting explicit analytic solutions with several of the desired features. In particular, the analytic solutions for the homogeneous turbulence models show the presence of two distinct time scales which characterize, respectively, the rapid settling of the tensor character of the flow to an asymptotic state and the slower development of the energy and mean scale. It is found that for both grid and homogeneous shear turbulence, the ratio of the two scales is about ten.

The fast time is the redistribution time, Λ/q, while the slower one is $b\Lambda/q$ (dissipation scale) for grid turbulence and $v'\Lambda/q$ (merging scale) for shear flows after an initial transient. This feature of the model solutions seems to be well reflected in the data.

V. RELATION BETWEEN THE HIGH REYNOLDS NUMBER DISSIPATION AND THE EDDY SIZE REARRANGEMENT

A further test of our modeling consists in comparing the spectra predicted by the R_{ij} model with experimental data. The simplest flow on which spectral information (Energy Spectra) is available is grid turbulence. A first cut at the analysis can be made by assuming that grid turbulence is isotropic (Ref. 5). This assumption is in fact not correct, and a more general framework is needed in order to understand the full details of the measurements. A remarkable result can be demonstrated, however. For high turbulence Reynolds numbers ($q\Lambda/\nu$ large), the energy dissipation is given experimentally by

$$\frac{\partial q^2}{\partial t} = -2b \frac{q^3}{\Lambda} \quad , \quad b \approx 0.125 \tag{87}$$

A theorem due to G.I. Taylor (Ref. 4, p. 100) states on the other hand that

$$\frac{\partial q^2}{\partial t} = -2\nu \frac{q^2}{\lambda^2} \tag{88}$$

The two statements of dissipation are equivalent if the following relation (Glushko, Ref. 6) is assumed

$$\lambda^2 = \frac{\Lambda^2}{a + b \frac{q\Lambda}{\nu}} \tag{89}$$

We demonstrate below that a simple model of eddy size rearrangement needed to obtain closure of the R_{ij} equation implies (89). We introduce wave number space by

$$\phi_{ij}(\vec{k}) = \frac{1}{8\pi^3} \int R_{ij}(\vec{r})\, e^{i\vec{k}\cdot\vec{r}}\, d\vec{r} \tag{90}$$

and the three-dimensional spectrum, E, by the Karman-Howarth relation

$$\phi_{ij}(\vec{k}) = \left(\delta_{ij} - \frac{k_i k_j}{k^2} \right) \frac{E(k)}{4\pi k^2} \tag{91}$$

---

5. Cerasoli, C., Donaldson, C.duP. and Sandri, G., "Fundamental Research in Turbulent Modeling," AFOSR TR-80-0324, February 1980.

6. Glushko, G.S., "Turbulent Boundary Layer on a Flat Plate in an Incompressible Fluid," Bull. Acad. Sciences USSR, Mech. Series No. 4, 1965, pp. 13-23.

The normalization is chosen so that

$$\frac{q^2}{2} = \int_0^\infty E(k)\, dk \tag{92}$$

The R_{ij} equation becomes

$$\frac{\partial E}{\partial t} = T(k) - 2\nu k^2 E \tag{93}$$

where the transfer function T which represents "cascading" (more properly, eddy size rearrangement) satisfies

$$\int_0^\infty T(k)\, dk = 0 \tag{94}$$

i.e., eddy size rearrangement does not change the energy. A simple model for T, which has derivatives only (no integrals) both in $\vec{k}$ space and for R_{ij}, is

$$T = -\frac{q}{\Lambda}\alpha\left[\frac{5}{3}E + k\frac{\partial E}{\partial k}\right] + \frac{2}{3}\frac{q}{\Lambda}\alpha\lambda^2 k^2 E \tag{95}$$

The coefficients have been chosen so that for Kolmogoroff equilibrium, i.e., $T = 0$, the only solution is

$$E = \text{const} \cdot k^{-5/3}$$

and, in addition, Eq. (94) is satisfied. For purposes of calculational feasibility, it is most desirable that the model equations be differential. If both ϕ_{ij} and R_{ij} are to be governed by differential equations, then it can be shown that all terms in the modeling of T must be of the form $a_n k^n \partial^n E/\partial k^n$. A general consequence of such assumptions is that $\phi(k)$ will exhibit a region where ϕ is proportional to a power of k. From the point of view of theory, it seems that the simplest assumption one can make on the eddy size rearrangement model is that it be local simultaneously in wave number and relative separation. To obtain Eq. (89), we consider a steady source at k_0

$$\frac{q}{\Lambda}\alpha\left[\frac{5}{3}E + k\frac{\partial E}{\partial k}\right] + 2\nu k^2 E\left[\frac{\alpha}{3}\text{Re}\,\frac{\lambda^2}{\Lambda^2} - 1\right] =$$

$$= Q_0\delta(k - k_0) \quad , \quad \text{Re} \equiv \frac{q\Lambda}{\nu} \tag{96}$$

The exact solution is

$$E = \frac{Q_o}{(q/\Lambda)\alpha k_o} e^{\kappa} H\left(\frac{k}{k_o} - 1\right) \frac{e^{-(k-k_c)^2\kappa}}{(k/k)^{5/3}} \tag{97}$$

with H the Heaviside function and

$$\kappa = \frac{k_o^2 \Lambda^2}{\alpha Re} - \frac{k_o^2 \lambda^2}{3} \tag{98}$$

We now impose, as integral constraints, the definitions of $q^2/2$, λ and Λ .

$$\frac{q^2}{2} = \int_0^\infty E(k)\, dk = E_o k_o I_1(\kappa) \tag{99}$$

$$\frac{q^2}{2} \frac{1}{\lambda^2} = \int_0^\infty k^2 E\, dk = E_o k_o^2 I_2(\kappa) \tag{100}$$

$$\frac{2}{\pi} \frac{q^2}{2} \Lambda = \int_0^\infty \frac{E}{k}\, dk = E_o I_3(\kappa) \tag{101}$$

where we have introduced three convenient integrals, I_1 , I_2 , I_3 , and the abbreviation

$$E_o = \frac{Q_o}{(q/\Lambda)\, k_o} e^{\kappa} \tag{102}$$

After some manipulation, we find

$$\frac{\Lambda^2}{\lambda^2} = \frac{e^{-\kappa}}{2 I_1(\kappa)} \alpha Re \tag{103}$$

Numerical evaluation of I_1 then gives

$$\lambda^2 \approx \frac{\Lambda^2}{(\pi^2/4) + (\alpha Re/3)} \tag{104}$$

Comparing Eq. (104) with (89), we obtain

$$a = \frac{\pi^2}{4} = 2.47 \ , \quad b = \frac{\alpha}{3} \tag{105}$$

It is interesting to note that the empirically accepted values of a lie between 3.25 and 2.5. We note here a general result, namely that a model of the eddy size rearrangement term in the R_{ij} equation determines the asymptotic model in the $\overline{u_i u_j}$ equation. This is not obvious when one merely considers the contraction of the R_{ij} equation into the $\overline{u_i u_j}$ equation. From dimensional arguments, it can be shown that a family of models should yield the Glushko relation and, in addition, that if the spectrum has the Kolmogoroff form

$$E \underset{Re\to\infty}{\longrightarrow} A\,\varepsilon^{2/3} k^{-5/3} \qquad \text{for} \quad k > k_o$$

then the dissipation parameter b is given by

$$b = \frac{\pi}{5 \cdot 3^{3/2}} A^{-3/2} = 0.121 A^{-3/2} \tag{106}$$

Experimentally, $A \approx 1$; thus Eq. (106) yields a value for b that is close to the generally accepted value of b, i.e., 0.125.

It is of interest to observe that a model in the sense of the familiar Krook model (or single relaxation time model) would not require any derivatives at all. Unfortunately, it does not seem possible to implement such a concept in modeling cascading because the "equilibrium" spectrum (assumed of Kolmogoroff form) has infinite dissipation.

VI. CONCLUSIONS

We have tested our formulation of the modeled equations for the R_{ij} tensor by illustrating its properties in the case of homogeneous turbulence. Our analysis of the model of homogeneous turbulence has brought out four main conclusions.

1. The model contains only two adjustable parameters which we chose to fix from grid turbulence data. Good qualitative agreement with homogeneous shear flow results.

2. The model implies the existence of two distinct time scales which are separated by a factor of about 10. They appear after an initial transient phase has died out during which q/Λ becomes approximately equal to U'. On the fast scale, $\Lambda/q \approx (U')^{-1}$, the normalized deviator

$$a_{ij} = \frac{\overline{u_i' u_j'}}{q^2} - \frac{1}{3}\delta_{ij}$$

locks into a constant value indicated by a Corrsin parameter (Refs. 7 and 8)

$$\frac{|\overline{u_1' u_2'}|}{\sqrt{\overline{u_1'^2}\;\overline{u_2'^2}}} \sim 0.5$$

or by a Bradshaw number

$$\frac{|\overline{u_1' u_2'}|}{q^2} \sim 0.19$$

On the slower scale, $v'(\Lambda/q) \sim 0.07(\Lambda/q)$, the energy components and the mean scale grow exponentially. This solution can be thought of as a superequilibrium with convection. A qualitative physical picture is as follows. During the initial transient, when $(q_0/\Lambda_0) \ll U'$, the shear brings the sudden distortion-like turbulence up to convective equilibrium ($q/\Lambda \approx U'$), while when $(q_0/\Lambda_0) \gg U'$, the turbulence decays grid-like to convective equilibrium. Then a merging mechanism takes over (a multi-layer Brown-Roshko effect) so that eddies fold with each other, making larger ones indefinitely (as long as the imposed shear provides the energy to sustain the process). Once the merging process takes over, the eddy structure remains fixed and exhibits highly directional integral scales (see 4 below).

7. Harris, V.G., Graham, J.A.H. and Corrsin, S., "Further Experiments in Nearly Homogeneous Turbulent Shear Flow," J. Fluid Mech. 81, 1977, pp. 657-687. Corrigendum, J. Fluid Mech. 86, 1978, pp. 795-796.

8. Corrsin, S. and Kollman, W., "Preliminary Report on Suddenly Sheared Cellular Motion as a Qualitative Model of Homogeneous Turbulent Shear Flow," Proc. SQUID Symposium on Turbulence in Internal Flows, pp. 11-33 (S.N.B. Murthy, ed.), Hemisphere Publishing Co., 1977

3. In the model, the two transverse energy components do not separate while the data indicate that such a separation occurs. The splitting can, however, be brought into the model by assuming a tensor coefficient in the redistribution equation. We have taken this point to constitute a refinement at this stage of analysis.

4. The calculated angular averaged integral scales are quite directional. The model thus gives a picture of the eddy structure of a sheared turbulence. With our choice of parameters

$$\frac{\Lambda_{11}}{\Lambda_{22}} \sim 2.6 \quad , \quad \frac{\Lambda_{12}}{3\Lambda} \sim 0.19$$

this picture could eventually be tested by experiment.

The derivation of the scale equation, the agreement of the model with homogenous shear flows, and the derivation of the Glushko relation are, in our opinion, strong arguments in support of developing a full model for R_{ij} .

APPENDIX A.

THE INTERCOMPONENT REARRANGEMENT MODEL FOR ISOTROPIC TURBULENCE

We prove that our modeling of the two-point intercomponent rearrangement term makes this term vanish automatically for isotropic turbulence. We also show why this statement is nontrivial for two-point as contrasted to one-point models.

The intercomponent rearrangement two-point tensor is given by

$$A_{ij}(\vec{x}_c,\vec{r}) = \left\langle p'(\vec{x}) \frac{\partial u_j'(\vec{y})}{\partial x_{ci}} + \frac{\partial u_i'(\vec{x})}{\partial x_{cj}} p'(\vec{y}) \right\rangle \tag{A.1}$$

We model generally A_{ij} as (Eq. (23) in the text)

$$A_{ij} \overset{M}{=} -\frac{q}{\Lambda}\left[R_{ij} - \frac{1}{3}\delta_{ij}R_{\alpha\alpha} + C_{ij}\right] \tag{a.2}$$

From the definition, Eq. (A.1) and the continuity relations

$$\frac{\partial u_i(\vec{x})}{\partial x_{ci}} = \frac{\partial u_i(\vec{y})}{\partial x_{ci}} = 0 \tag{A.3}$$

we find that A_{ij} must be traceless; i.e.,

$$A_{kk} = 0 \tag{A.4}$$

From Eq. (A.4) we conclude that C_{ij} itself must be traceless. In fact,

$$0 = A_{kk} = -\frac{q}{\Lambda}\left[R_{kk} - R_{\alpha\alpha} + C_{kk}\right] = -\frac{q}{\Lambda}C_{kk} \tag{A.5}$$

For homogeneous turbulence, R_{ij}, C_{ij} and hence A_{ij} depend on the separation $\vec{r}$ only. We Fourier transform Eq. (A.2) with respect to $\vec{r}$ using Eq. (90) and analogous equations to define $\tilde{A}_{ij}$ and $\tilde{C}_{ij}$. We find in wave number space

$$\tilde{A}_{ij}(\vec{k}) = -\frac{q}{\Lambda}\left[\phi_{ij}(\vec{k}) - \frac{1}{3}\delta_{ij}\phi_{\alpha\alpha} + \tilde{C}_{ij}(\vec{k})\right] \tag{A.6}$$

For all the models that we consider for isotropic turbulence, S_{ij} satisfies continuity automatically. We can then determine C_{ij} uniquely. In fact, from isotropy the most general symmetric second rank tensor can be written in terms of two scalars, $a(k)$ and $b(k)$ as

$$\tilde{C}_{ij}(\vec{k}) = a(\vec{k})\delta_{ij} + b(k)\hat{k}_i\hat{k}_j \tag{A.7}$$

where $\hat{k}$ denotes the unit vector

$$\hat{k}_i = k_i/k \tag{A.8}$$

But $\tilde{C}_{ij}$ is traceless by Eq. (A.5); thus, from Eq. (A.7)

$$0 = 3a + b \tag{A.9}$$

Substituting (A.9) into (A.2), we have

$$\tilde{C}_{ij}(\vec{k}) = a(k)\left[\delta_{ij} - 3\hat{k}_i\hat{k}_j\right] \tag{A.10}$$

Continuity of A_{ij} requires

$$\begin{aligned} 0 &= k_i A_{ij} \\ &= -\frac{q}{\Lambda} k_i \left[\phi_{ij}(\vec{k}) - \frac{1}{3}\delta_{ij}\phi_{\alpha\alpha} + \tilde{C}_{ij}\right] \\ &= -\frac{q}{\Lambda} k_j \left[-\frac{1}{3}\phi_{\alpha\alpha} - 2a(k)\right] \end{aligned} \tag{A.11}$$

Hence $a(k)$ is determined:

$$a(k) = -\frac{1}{6}\phi_{\alpha\alpha} = -\frac{1}{12\pi}\frac{E(k)}{k^2} \tag{A.12}$$

and from Eq. (A.10), C_{ij} is determined uniquely by the energy spectrum

$$\tilde{C}_{ij}(\vec{k}) = -\frac{1}{6}\phi_{\alpha\alpha}(k)\left[\delta_{ij} - \hat{k}_i\hat{k}_j\right] \tag{A.13}$$

We now substitute (A.13) into (A.6) and use the Karman-Howarth theorem, Eq. (91) in the form

$$\phi_{ij}(\vec{k}) = \left(\delta_{ij} - \hat{k}_i\hat{k}_j\right)\frac{\phi_{\alpha\alpha}}{2} \tag{A.14}$$

We find

$$\begin{aligned} \tilde{A}_{ij}(\vec{k}) &= -\frac{q}{\Lambda}\left[\left(\delta_{ij} - \hat{k}_i\hat{k}_j\right)\frac{\phi_{\alpha\alpha}}{2} - \frac{1}{3}\delta_{ij}\phi_{\alpha\alpha} - \left(\delta_{ij} - 3\hat{k}_i\hat{k}_j\right)\frac{\phi_{\alpha\alpha}}{6}\right] \\ &= 0 \end{aligned} \tag{A.15}$$

This completes the proof of our theorem.

If we had assumed a model for A_{ij} without the C_{ij} term, i.e.,

$$A_{ij} \overset{M'}{=} -\frac{q}{\Lambda}\left[R_{ij} - \frac{1}{3}\delta_{ij}R_{\alpha\alpha}\right] \tag{A.16}$$

we would have violated the requirement that A_{ij} vanish for isotropic turbulence because (in $\vec{r}$ space), using the Karman-Howarth representation

$$R_{ij} = \frac{q^2}{3}\left[g\delta_{ij} + (f-g)\hat{r}_i\hat{r}_j\right] \tag{A.17}$$

We find

$$R_{ij} - \frac{1}{3}\delta_{ij}R_{\alpha\alpha} = \frac{q^2}{18}\left(\delta_{ij} - 3\hat{r}_i\hat{r}_j\right) r\, f'(r) \neq 0 \tag{A.18}$$

Following von Karman and Howarth, we have considered here only mirror symmetric isotropic turbulence and hence neglected the skew-symmetric part of R_{ij} (and of C_{ij}). A straightforward calculation, which follows essentially the steps given here, shows that the skew-symmetric parts of ϕ_{ij} and $\tilde{C}_{ij}$

$$\underset{\sim}{\phi}_{ij} = \epsilon_{ij\alpha}\hat{k}_\alpha A(k) \quad , \quad \underset{\sim}{\tilde{C}}_{ij} = \epsilon_{ij\alpha}\hat{k}_\alpha c(k) \tag{A.19}$$

are related by

$$A(k) + c(k) = 0 \tag{A.20}$$

in order to satisfy the theorem. The result is therefore valid for general isotropic turbulence.

Mathematically we may summarize our analysis in the following theorem:

> Any isotropic (second rank) tensor that is traceless and divergence-free is skew-symmetric (and therefore a curl).

Even though it is possible that alternative models satisfy the isotropy requirement, i.e., $A_{ij} = 0$, it is an advantage of the model proposed here that it does so explicitly.

A.R.A.P. Report 438

FUNDAMENTAL RESEARCH IN TURBULENT MODELING

PART 2. EXPERIMENT

by

Carmen Cerasoli
and
Guido Sandri

TABLE OF CONTENTS

Part 2. Experiment

I. INTRODUCTION

The study of turbulent flows began over a century ago with the work of Reynolds. Since that time, our understanding of turbulent flows has grown, but not as rapidly or dramatically as in many other fields of science. A very old and useful concept in the study of turbulence is the turbulent length scale, or, more physically, the "eddy" size. The notion of a typical eddy size is intimately connected with the turbulent transport of all flow variables, and is an aid in qualitatively understanding turbulent flows. The concept of length scale enters explicitly when one attempts to simulate turbulent flows numerically by use of "second order closure" models. Data on the magnitude of the turbulent scales is required as input for such modeling schemes, and the present experimental study provides data on turbulent scales for an annular flow field.

The manner in which length scales appear in closure models will be discussed in Section II. We will also present the definition of the correlation tensor and the way in which length scales can be defined via this tensor. The experimental facilities and techniques used here will be discussed in Section III, while data on the basic flow field (mean and turbulent velocities) will be presented in Section IV. Section IV will also include a discussion of theoretical concepts related to the mean and turbulent velocity fields, and a comparison of our data with that from previous experiments. Turbulent length scales obtained by use of auto-correlation measurements and Taylor's hypothesis are presented in Section V, where, again, theory and experiment are discussed. The notion of the von Karmon length scale is also introduced and compared to data.

Section VI contains results obtained from two-point correlation measurements, and data are compared to previous experiments and our theoretical knowledge. In particular, results are discussed using concepts developed for isotropic and homogeneous flows. Although the annular flow field is neither isotropic nor homogeneous globally, these concepts are useful and consistent with our data in certain spatial regions where the mean flow gradients are small.

The two-point correlation equations are also presented, and we qualitatively discuss the effect of the production terms on the various correlation functions. The results from this study are summarized in Section VII and future research topics are discussed.

II. SECOND ORDER CLOSURE MODELS AND THE CORRELATION TENSOR

The typical method for solving turbulent flows requires the decomposition of dependent flow variables into mean and fluctuating parts. The total velocity field is written as

$$U_i + u_i$$

where U_i is the mean velocity (either a time or ensemble average) and u_i is the fluctuating part; the subscript i runs from 1 to 3 for the three velocity components. A similar separation is used for all other dependent variables, such as temperature, density, etc. The following equations result when such a decomposition is applied to the Navier-Stokes equations for incompressible, constant temperature flow:

$$\frac{\partial U_i}{\partial t} + U_j \frac{\partial U_i}{\partial x_j} + \frac{1}{\rho}\frac{\partial P}{\partial x_i} - \nu\nabla^2 U_i = \frac{\partial}{\partial x_j}\left(\overline{u_i u_j}\right)$$

where P and ρ are the mean pressure and density, respectively, ν is the kinematic viscosity, repeated indices are summed over and the overbar denotes an average. We find that the equation for mean variables involves the correlation of fluctuating variables, $\overline{u_i u_j}$. The equation for $\overline{u_i u_j}$ reads

$$\frac{\partial}{\partial t}\overline{u_i u_j} + U_k \frac{\partial}{\partial x_k}\overline{u_i u_j} = -\overline{u_i u_k}\frac{\partial U_j}{\partial x_k} - \overline{u_j u_k}\frac{\partial U_i}{\partial x_k} - \frac{\partial}{\partial x_k}\left(\overline{u_i u_j u_k}\right) - \frac{\partial}{\partial x_i}\left(\overline{p u_j}\right)$$
$$- \frac{\partial}{\partial x_j}\left(\overline{p u_i}\right) + \overline{p\left(\frac{\partial u_i}{\partial x_j} + \frac{\partial u_j}{\partial x_i}\right)} + \nu\frac{\partial^2}{\partial x_k^2}\overline{u_i u_j} - 2\nu\overline{\frac{\partial u_i}{\partial x_k}\frac{\partial u_k}{\partial x_j}}$$

Here we find that the equation for the second order quantity, $\overline{u_i u_j}$, involves third order variables, $\overline{u_i u_j u_k}$, pressure-velocity correlations, $\overline{p u_j}$, and pressure-velocity gradient terms, $\overline{p(\partial u_i/\partial x_j)}$. One can continue this process and the equation for third order variables will involve fourth order terms. This problem of always having one equation less than the number of dependent variables is the "closure" problem. The equations can be closed at the first order by writing $\overline{u_i u_j}$ as a function of the mean, or first order, variables. This is usually done via the concept of an eddy viscosity, ν_E, such that

$$\overline{u_i u_j} = \frac{q^2}{3}\delta_{ij} + \nu_E \left(\frac{\partial U_i}{\partial x_j} + \frac{\partial U_j}{\partial x_i}\right)$$

where

$$q^2 = u_i u_i$$

and

$$\delta_{ij} = 1 \qquad i = j$$
$$= 0 \qquad i \neq j$$

This method essentially treats turbulent mixing in a manner similar to viscous diffusion and can yield reasonable results for certain flow fields. The next level of sophistication is to close the system at second order, and this allows the physics of turbulence to be more accurately modeled than the use of eddy viscosities. The set of equations are closed at second order by writing equations for $\overline{u_i u_j u_k}$, $\overline{pu_i}$ and $\overline{p(\partial u_i/\partial x_j)}$ solely in terms of second order quantities. The present A.R.A.P. model uses the following equations:

$$\overline{u_i u_j u_k} = - V_c \Lambda q \left[\frac{\partial}{\partial x_k}(\overline{u_i u_j}) + \frac{\partial}{\partial x_i}(\overline{u_j u_k}) + \frac{\partial}{\partial x_j}(\overline{u_i u_k})\right]$$

$$\overline{pu_i} = - P_c \rho \Lambda q \frac{\partial}{\partial x_j}(\overline{u_i u_j})$$

$$\overline{p\frac{\partial u_i}{\partial x_j}} + \overline{p\frac{\partial u_j}{\partial x_i}} = - \frac{\rho q}{\Lambda}\left(\overline{u_i u_j} - \frac{q^2}{3}\delta_{ij}\right)$$

where the constants V_c and P_c are determined experimentally. The symbol Λ represents a variable length which is locally representative of the integral turbulent length scale, or alternately, a typical eddy size.

The determination of Λ requires knowledge of the correlation tensor, defined as

$$\tilde{R}_{ij}\ (\underline{r};\ \Delta\underline{r}) \equiv \overline{u_i(\underline{r})\ u_j(\underline{r} + \Delta\underline{r})}$$

For the case $\Delta r = 0$, $\tilde{R}_{ij}\ (\underline{r};\ 0)$ equals the turbulent intensity squared for each velocity component when $i = j$, and the turbulent shear stress when $i \neq j$. $\tilde{R}_{ij}(\underline{r},\ \Delta\underline{r})$ will in general be a function of the vector position $\underline{r}$ within the flow field and the vector separation $\Delta\underline{r}$. A normalized version of $\tilde{R}_{ij}$ will be used in most of this work, defined as

$$R_{ij}(\underline{r};\ \Delta\underline{r}) = R_{ij}(\underline{r};\ \Delta\underline{r}) \Big/ \left[\overline{u_i(\underline{r})^2}\right]^{1/2}\left[\overline{u_i(\underline{r})^2}\right]^{1/2}$$

Correlation lengths may be generated from R_{ij} in a number of ways. One method is to first perform an angular average over all separation directions; this is known as a "Batchelor average" and is defined by

$$\left\langle R_{ij}(\underline{r};\ \Delta r)\right\rangle_B \equiv \iint_{\Omega} R_{ij}(\underline{r};\ \Delta\underline{r})\ d\underline{\Omega}$$

where $d\underline{\Omega}$ is the solid angle vector. A length scale may be defined by integrating over the scalar separation variable Δr,

$$L_{ij}(\underline{r}) \equiv \int_0^{\infty} \left\langle R_{ij}(\underline{r};\ \Delta r)\right\rangle_B\ d(\Delta r)$$

Note that one may generate nine independent length scales which are functions of position $\underline{r}$, and that L_{ij} is a tensor. Another way to define length scales is to integrate over a single separation direction while holding the other two separations at zero. We take a case using cylindrical coordinates as an example where

$$r = (r,\ \phi,\ z)$$

and

$$\underline{r} = (\Delta r,\ \Delta\phi,\ \Delta z)$$

Let $\Delta r = \Delta\phi = 0$, and a length scale $\Lambda_{ij,\ z}$ can be defined as

$$\Lambda_{ij,z} \equiv \int_0^\infty R_{ij}(\underline{r};\, o,o,\Delta z)\, d(\Delta z)$$

where the subscripts indicate the tensor component and the integration direction, respectively. Note that $\Lambda_{ij,k}$ is not a tensor and the subscripts are used purely for bookkeeping purposes. A total of 27 length scales can be defined by the preceeding technique (9 components times 3 directions). Second order closure models typically require a single length scale, and the richness of information contained in R_{ij} and its associated scales must be replaced by a single number. This is best done when one understands the structure and details of the correlation tensor.

The present study involves axisymmetric, annular flow and cylindrical coordinates are used, where (r,ϕ,z) are the radial, azimuthal and axial coordinates. The corresponding velocity components are $(u,v,W + w)$, where we have used the fact that the mean radial and azimuthal velocities are negligible and taken as zero $(U = V = 0)$. The flow is assumed to be well developed and axisymmetric, so R_{ij} is independent of ϕ and z, and we write R_{ij} as

$$R_{ij}\,(r;\, \Delta r,\Delta\phi,\Delta z)$$

Azimuthal separations were held to zero in all experiments, and either $\Delta r = 0$, $\Delta z \neq 0$, or $\Delta r \neq 0$, $\Delta z = 0$, so that the separations were either pure axial or pure radial. The axial separations were implied by use of Taylor's hypothesis which will be subsequently discussed. The axisymmetric nature of this flow results in

$$\overline{v_1 u_2} = \overline{u_1 v_2} = \overline{v_1 w_2} = \overline{v_2 w_1} = 0$$

where the subscripts refer to position,

$$1 = \underline{r}$$

$$2 = \underline{r} + \Delta\underline{r}$$

We therefore have a tensor with 5 independent, non-zero components for the annular flow field.

III. EXPERIMENTAL APPARATUS AND TECHNIQUES

The wind tunnel used in this study is described in a previous A.R.A.P. Report (Ref. 1), and a brief description of the facility will be given here for completeness. The facility is shown schematically in Figure (1), where the test section is an annulus with inner and outer radii, R_I and R_O, of 2.54 and 21.59 cm, respectively. The distance from the end of the contraction section to the test section can be varied by the addition or subtraction of cylindrical sections, and the minimum and maximum distances can be varied from 15 to 45 diameters ($2R_O$). The contraction section admits air through the region shown in Figure (1) and vanes are situated to direct the incoming air. The vanes may be set at any angle from 0^0 to 45^0, and when the vane angle is non-zero, angular momentum is imparted to the incoming air. The contraction process will then create a swirling flow in the annulus. A constant speed motor was used in conjunction with a variable speed fan drive to provide flow through the tunnel, and the mean axial velocity could be varied between approximately 1200 and 3000 cm/sec. Before discussing the data acquisition techniques, we will discuss certain problems associated with the wind tunnel.

Initial measurements made by this author showed that the flow field was highly unsteady. This was apparent in the behavior of the turbulent velocity power spectra as low frequencies were approached ($f \to 0$). Typically, as $f \to 0$, the power spectral density approaches a constant value which can be used to define a turbulent length scale. Our initial experiments showed a divergent behavior where the spectral level increased as $f \to 0$, and this indicated a high degree of unsteadiness.

The source of unsteadiness was traced to the inlet section. Initially, a fine screen was placed around the inlet and did not provide any damping of atmospheric motions. Such motions would be amplified as the flow contracted and gave rise to the unsteadiness; the problem was remedied by placing a 5 cm thick piece of polyurethane foam around the inlet section. This provided a pressure drop across the foam of more than 10 times the dynamic pressure based on the inlet velocity ($\rho U_I^2/2$, ρ is the fluid density and U_I is the inlet velocity), and filtered out all the atmospheric motions.

A detailed survey of the mean and turbulent velocity fields was taken following the solution of the unsteadiness problem. These measurements revealed that the flow field was not axisymmetric. One indication of this lack of symmetry was that the maximum mean axial velocity was at $r = .55R_O$ on the near side of the inner tube ($\phi = 0^0$), while the maximum mean occurred at $r = .35R_O$ on the far side of the inner tube ($\phi = 180^0$). This behavior was believed to be associated with the shape of the contraction section, which may have caused the flow

---

1. Bilanin, Alan J., Snedeker, Richard S., Sullivan, Roger D., and Donaldson, Coleman duP., "Final Report on an Experimental and Theoretical Study of Aircraft Vortices," AFOSR-TR-75-0664, A.R.A.P. Report No. 238, February 1975.

to become separated. The problem was remedied by placing three sections of honeycomb after the contraction section, as shown in Figure (2). The pressure drop associated with the honeycomb was great enough to reduce the asymmetries created in the contraction section, and data showed that the flow was symmetric to within our resolving capabilities. The disadvantage of this solution was that swirl cannot be introduced by the vanes. Swirl now must be introduced after the honeycomb in the annulus region, or the contraction section must be redesigned to eliminate the asymmetries. The solution of using honeycomb was the quickest and most inexpensive one, and enabled us to make a very complete set of measurements on non-swirling annular flow.

Fluid velocities were measured using hot film X probes which allowed parallel and traverse velocities to be determined. The probes were manufactured by Thermo Systems Incorporated (TSI, model number 1240-20), and the sensor elements were .05 mm in diameter and 1 mm long. TSI anemometers and linearizers (model 1054) were used in conjunction with the X probes. A variety of probe holders were designed and used in this study, but only two need to be described. The first probe holder allowed a single probe to be traversed radially on either side of the inner tube. This was used to obtain mean and turbulent velocities as a function of radius and determine the symmetry of the flow field. A TSI sum and difference amplifier (model 1063) was used during the single probe measurements. This provided output voltages which were in proportion to the parallel (sum) and transverse (difference) velocities. The second probe holder allowed one probe to remain at the fixed radius, r_F, while a second probe was traversed to other radii. This allowed two-point correlations to be measured for the case of pure radial separations. No sum and difference amplifiers were used in the two probe measurements as the signals were added and subtracted in the data analysis programs. The signals from the anemometer and linearizer units were amplified by AC coupled amplifiers with a bandwidth from 2Hz to over 20,000Hz. These amplified signals were transmitted via cable to the computer facility and into a low pass filter.

The filtered output was digitized by use of an analog to digital (A/D) converter. Digitized data was then stored on tape and subsequently analyzed. The sample rate for the single probe experiments was 5,000 samples a second, which gave a Nyquist frequency of 2,500Hz. The cutoff frequency for the low pass filter was 2,000Hz and this eliminated any sorce of aliasing error. The two probe measurements used the A/D converter in the multiplex mode. The sample rate for all four data channels was 50,000 samples per second, which yielded a sample rate per channel of 12,500Hz and a Nyquist frequency of 6250Hz; the low pass cutoff frequency was 5,000Hz. The data aquisition system is shown schematically in Figure (3), where the flow of data from probes and anemometers through amplifiers and filters, into the A/D converter and eventually to storage on tape can be seen. Computer programs were used to calculate mean velocities, RMS fluctuations, autocorrelations, power spectra and correlation functions.

All experiments were conducted with a maximum axial velocity of 1960 cm/sec and a mass flow velocity, W_B, (defined in Section IV) of 1660 cm/sec. The flow Reynolds based on mass flow velocity and the hydraulic diameter, $d_h = 2(R_O - R_I)$, was

$$R_e = \frac{W_B\, d_h}{\nu} = 4.2 \times 10^5$$

while the distance from the last section of honeycomb to the test section, z, was

$$z = 30\, D_o = 34\, d_h$$

Three sets of measurements were made for the two point correlations, where the fixed probe positions were $r_F = .27, .43$ and $.75$. (Note that from this point, all distances will be normalized by R_o .) These three positions were chosen because the mean axial velocity gradient (dW/dr) was positive, zero and negative, respectively, at these positions. Such measurements enabled us to examine the effect of mean shear and geometry on the correlation functions.

IV. MEAN AND TURBULENT VELOCITY MEASUREMENTS

A series of single probe measurements were made to map out the mean and fluctuating velocities in the annulus. The following variables were measured as a function of radial position: the mean axial or downstream velocity, W, the turbulent intensities for the radial, azimuthal, and axial velocities, u, v, w [= $(\overline{u^2})^{1/2}$, $(\overline{v^2})^{1/2}$, $(\overline{w^2})^{1/2}$], and the turbulent shear stress, $\overline{uw}$.

A. Mean Velocity

Figure 4 shows the mean axial velocity versus radius where velocities have been normalized by the mass flow, or bulk, velocity, W_B, defined as

$$W_B = \frac{1}{\pi(R_o^2 - R_o^2)} \int_0^{2\pi} \int_{R_I}^{R_o} W(r) r dr \, d\phi$$

R_I and R_o are the inner and outer radii, respectively. Measurements were made on each side of the center tube (denoted as "near" and "far" side) and W is symmetric to within the accuracy of the measurements. It is well known that the velocity can be represented logarithmically for the outer region in pipe flow (distance away from wall greater than $.05R_o$), and a similar behavior exists for the present case. Figure 5 shows the axial velocity versus distance from wall in semi-log coordinates, where the upper and lower graphs are for distances away from the inner and outer radial walls, respectively. Both cases show good logarithmic fits until the central annular region is approached; the velocities fall under the log profile for distances from the inner radial wall and are above the log profile for distances from the outer radial wall. No analytical solutions exist for this annular flow, therefore no comparisons can be made between theory and experiment. In the pipe flow case, the log profile is an excellent fit right to $r = 0$, the zero mean gradient position (Nikuradse, Ref. 2). The present case shows deviations from the log profile near the zero gradient position, $r = .43$, but one must be cautious when relating the behavior at $r = 0$, $dW/dr = 0$ in pipe flow to that at $r \neq 0$, $dW/dr = 0$ in annular flow. The point $r = 0$ is very different geometrically from a point such as $r = .43$.

B. Turbulent Intensities

The root mean square turbulent velocities are presented in Figure 6 as a function of radius. The velocities were normalized by the bulk velocity and the data are from near side measurements. As in the case for the mean axial velocity, near and far side turbulent intensities agreed to within measurement accuracy. A number of features can be discussed in terms of our general

---

2. Nikuradse, J., "Gesetzmäbigkeit der Turbulenten Strömung in Glatten Rohren," Forsch. Arb. Ing.-Wes. No. 356, 1932.

knowledge of turbulent shear flows. In the regions away from the zero gradient position ($r = .43$), we have $w > v \simeq u$. This is a common feature where the velocity component receiving energy by production directly (w) is greater than the other two components. The velocity component perpendicular to the gradient direction (v) is greater than the component parallel to the gradient direction (u); similar behavior is observed and discussed by Champagne et.al. (Ref. 3). The parabolic behavior of $w(r)$ is consistent with pipe flow measurements and w is a minimum at the zero gradient position where no local production occurs. Two features of the data differ from expectations. The first is the "bulge" in the w profile near $r \simeq .65$. This is a reproducible feature and we can offer no explanation for it as no anamolous behavior occurs in other flow variables near this position. The second feature is the lack of isotropy at the zero gradient position, that is, $w \neq u = v$ at $r = .43$, and we define an isotropy factor $\gamma \equiv (u/w)_{r=.43} = .72$. Note that the measured values for the transverse velocities (u and v) were corrected for the effects of tangential cooling (see Appendix A). Had this not been done, the isotropy factor would have been even lower. The degree of tangential cooling is embodied in the k factor, which was measured for the hot film probes used here. The values agree with the published results of Frieke and Schwarz (Ref. 4) and Jorgensen (Ref. 5), but a fair amount of scatter exists in all the measurements. If we take the largest k measured (which results in the greatest correction factor), the isotropy factor is increased to about .78, as opposed to .72. This lack of isotropy may be a consequence of the flow field not being fully developed. Priest (Ref. 6) shows data on the evolution of w and u downstream in pipe flow, and there is a tendency for w to become independent of downstream distance before u (and v). Priest's results show that at $r = 0$,

$\gamma = .70$	$z/D = 20$
$\gamma = .76$	$z/D = 30$
$\gamma = .78$	$z/D \geq 45$

The present result concerning isotropy can be compared to pipe flow measurements at $r = 0$, and the values of γ are summarized below.

---

3. Champagne, F. H., Harris, V. G. and Corrsin, S., "Experiments on Nearly Homogeneous Turbulent Shear Flow," J. Fluid Mech. 41, pp. 81-139.
4. Frieke, C. A. and Schwarz, W. H., "Deviations from the Cosine Law for Yawed Cylindrical Anemometer Sensors," J. Applied Mech., Dec. 1968, pp. 655-662.
5. Jorgensen, F. E., "Directional Sensitivity of Wire and Fiber-film Probes," Disa Report No. 11, May, 1971, pp. 31-37.
6. Priest, A. J., "Incompressible Turbulent Flow in Pipes and Conical Diffusers," Ph.D Thesis, University of Salford, England, 1975.

Annular Flow r = .43	Pipe Flow = 0		
Present Experiment	Laufer(Ref. 7)	Priest(Ref. 6)	Sabot and Comte-Bellot(Ref. 8)
.72	.98	.78	.90

Typical error bounds on γ are about .04, so that substantial disagreement exists in the literature concerning the degree of anisotropy at pipe center. All three pipe flow measurements were made at downstream distances greater than 90 pipe diameters, and lack of fully developed flow is not responsible for the differences. It is not clear whether the various authors corrected the data for tangential cooling, and if this is the cause for the differences. The reader should note that a similar problem exists in circular jet measurements. Wygnanski and Fiedler (Ref. 9) found $\gamma = .86$ on jet centerline (and does compensate for tangential cooling), while Gibson (Ref. 10) found perfect isotropy, $\gamma = 1$, on centerline.

C. Turbulent Shear Stress

Measurements of the turbulent shear stress, $\overline{uw}$, and the shear stress coefficient, $\overline{uw}/(\overline{u^2})^{1/2}(\overline{w^2})^{1/2}$, were made as a function of radius. These measurements are sensitive to both probe calibration and orientation, and this can be seen by noting that

$$\overline{uw} \sim \overline{(e_A - e_B)(e_A + e_B)} = \overline{e_A^2} - \overline{e_B^2}$$

where e_A and e_B are the fluctuating voltages from sensors A and B of an X wire probe. If (1) the sensitivities of the two sensors are not equal, or (2) the probe axis is not parallel to the mean flow direction, the measured value of $\overline{uw}$ will be in error. Such errors can be substantially reduced by appropriately averaging two measurements where the probe is rotated 180° about its axis, thereby interchanging the positions of sensors A and B. This procedure was used and results for the shear stress coefficient are presented in Figure 7. Measurements from the near and far sides are shown and the degree

---

7. Laufer, J., "The structure of Turbulence in Fully Developed Pipe Flow," N.A.C.A. Report No. 1174, 1954.
8. Sabot, J. and Comte-Bellot, G., "Intermittency of Coherent Structures in the Core Region of Fully Developed Turbulent Pipe Flow," J. Fluid Mech. 74, 1976, pp. 767-96.
9. Wygnanski, I. and Fiedler, H., "Some Measurements in the Self-Preserving Jet," J. Fluid Mech. 38, 1969, pp. 577-612.
10. Gibson, M. M., "Spectra of Turbulence in a Round Jet," J. Fluid Mech. 15, 1963, pp. 161-73.

of asymmetry is the same order as the experimental uncertainties. The values of approximately 0.4 in the constant coefficient regions are in good agreement with the value of 0.4 given by Laufer for pipe flow. The shear stress coefficient is zero at $r \approx .43$, where the mean gradient is zero, and the sign change in the coefficient relates to the sign change in dW/dr. The shear stress is presented in Figure 8, where we have averaged the near and far side data. The dashed line represents a fit to a theoretical expression for $\overline{uw}$ which we will now discuss.

The derivation for $\overline{uw}$ as a function of radius in pipe flow is a textbook exercise which can be found in Fluid Dynamics by Daily and Harleman (Ref. 11). The derivation requires the assumption of well developed flow, and when applied to the case of annular flow gives

$$\overline{uw} = \frac{Ar}{R_o} - \frac{BR_o}{r} + \nu \frac{dW}{dr}$$

$$A = \frac{1}{R_o^2 - R_I^2} \left[R_o^2 \, u_{*,o}^2 + R_o R_I \, u_{*,I}^2 \right]$$

$$B = \frac{1}{R_o^2 - R_I^2} \left[R_I^2 \, u_{*,o}^2 + R_o R_I \, u_{*,I}^2 \right]$$

$$u_{*,o}^2 = \nu \left. \frac{dW}{dr} \right|_{r=R_o} \qquad u_{*,I}^2 = \nu \left. \frac{dW}{dr} \right|_{r=R_I}$$

$u_{*,I}$ and $u_{*,o}$ are friction velocities based on the mean gradient at the inner and outer radii. The variable r in the above expressions is the dimensional radius, as this allows one to see how R_o and R_I appear in the equations. The case $R_I = 0$ yields

$$A = u_{*,o}^2 = u_*^2$$

$$B = 0$$

and

$$\overline{uw} = u_*^2 \frac{r}{R_o} + \nu \frac{dW}{dr}$$

which is the well known result for pipe flow. The friction velocities can be related to the downstream pressure gradient by

---

11. Daily, J. W. and Harleman, D. R. F., Fluid Dynamics, Addison-Wesley Publishing Co., 1966.

$$\frac{1}{\rho}\frac{\partial P}{\partial z} = -\frac{1}{R_o^2 - R_I^2}\left[R_o^2\, u_{*,o}^2 + R_I^2\, u_{*,I}^2\right]$$

and the expression reduces to the pipe flow result for $R_I = 0$.

The theoretical expression for $\overline{uw}$ involves two constants, $u_{*,o}$ and $u_{*,I}$, which can be obtained by direct measurement. Boundary layer measurements were not made to determine gradients at the walls and, as a consequence, the following methodology will be considered. The position at which $\overline{uw} = 0$ can be used to determine the ratio of $u_{*,o}$ to $u_{*,I}$, and using $\overline{uw} = 0$ at $r = .43$, we find

$$\frac{u_{*,I}}{u_{*,o}} = 1.33$$

$$\overline{uw} = u_{*,o}^2\left[1.227\,\frac{r}{R_o} - .227\,\frac{R_o}{r}\right] + \nu\frac{dW}{dr}$$

The experimental data can be fit to the above expression and yields $u_{*,o} = .033\ W_B$. Alternately, the friction velocity can be computed from measured values of dP/dz (again using $u_{*,I} = 1.33\ u_{*,o}$), which gives $u_{*,o} = .040\ W_B$. Finally, the data of Koch and Feind (Ref. 12) show $u_{*,o} = .039\ W_B$ for annuli with $R_I/R_o = .6$ and .8. These three values are summarized below.

$u_{*,o}/W_B$	Technique	
.033	Fit Shear Stress Data to Theory	Present Study
.040	Pressure Gradient Measurement	Present Study
.039	Koch and Feind	

The fit to data yields a $u_{*,o}$ below that of the other two values, although a better agreement can be obtained by choosing a higher k factor for the tangential cooling. The largest reasonable value of k (as previously discussed) gives $u_{*,o} = .036\ W_B$, which agrees with the other values to within experimental uncertainties. The experimental values of $\overline{uw}$ tend to be less than theoretically predicted as the inner radius is approached, and this may be a consequence of the flow not being fully developed.

This concludes the discusssion of the mean and turbulent flow variables. The flow is symmetric to within our resolving capability, and the general features

---

12. Koch, R. and Feind, K., "Druckverlust und Wärmeübergang in Ringspalten," Chemie-Ing.-Techn., 30, 1958, pp. 577-84.

of the flow agree with our knowledge of turbulent shear flow. The mean velocity profile is logarithmic, while the turbulent intensities have a parabolic behavior with minimum values near the midpoint between the inner and outer radii. The behavior of the shear stress coefficient agrees well with past experiments, while $\overline{uw}$ agrees reasonably well with the theoretical prediction. Certain details of the experiment do not precisely agree with theory and expectations and this is probably a consequence of the flow not being completey developed.

V. TURBULENT LENGTH SCALES VIA TAYLOR'S HYPOTHESIS

Turbulent length scales can be obtained using single point autocorrelation measurements in conjunction with Taylor's hypothesis. That is, the following correspondence can be made,

$$R_{uu}(\Delta z) = W \; R_{uu}(\tau)$$

where

$$\overline{u^2}\, R_{uu}(\tau) \equiv \lim_{T\to\infty} \frac{1}{2T} \int_{-T}^{+T} u(z,t)\, u(z,t+\tau)\, dt$$

$$\overline{u^2}\, R_{uu}(\Delta z) \equiv \lim_{T\to\infty} \frac{1}{2T} \int_{-T}^{+T} u(z,t)\, u(z+\Delta z,t)\, dt$$

$$\overline{u^2} \equiv \lim_{T\to\infty} \frac{1}{2T} \int_{-T}^{+T} {}^{2}(z,t)\, dt$$

and W is the local downstream velocity. The correlation functions are independent of z and t for fully developed flows. Taylor's hypothesis essentially states that the eddy field is frozen and convected downstream by the local mean velocity. Two criteria are necessary for this assumption to be valid, (1) the turbulent intensity must be low,

$$W >> w$$

and (2) the mean flow gradients must be small relative to a typical cross section stream eddy size, ℓ

$$1 >> \frac{\ell}{W}\frac{dW}{dr}$$

These two criteria are well satisfied in the central annular region where mean gradients and turbulent intensities are low,

$$r = .25 \text{ to } .75 \qquad w \lesssim .06\, W$$

$$\frac{dW}{dr} \lesssim .08\, \frac{W}{\ell}$$

These criteria are not as well satisfied near the inner and outer radii, but probably do not invalidate the use of Taylor's hypothesis. The worst case values are

$$w \simeq .12\ W$$

and

$$\frac{dW}{dr} \simeq .2\ \frac{W}{\ell}$$

The autocorrelation can be used to define integral length scales by

$$\Lambda_{uu,z} \equiv W \int_0^{\tau_0} R_{uu}(\tau)\ d\tau$$

where τ_0 is the position of the first zero in $R_{uu}(\tau)$; this convention of integrating to τ_0 is a standard one and is discussed in Hassan et. al. (Ref. 13). The $\Lambda_{uu,z}$ notation is one in which the first two subscripts refer to the correlation function indices, while the last index refers to the integration direction (downstream in this case, by Taylor's hypothesis). The following integral scales, $\Lambda_{uu,z}$, $\Lambda_{vv,z}$ and $\Lambda_{ww,z}$ were obtained as a function of radius and are presented in Figure (9). The behavior of $\Lambda_{uu,z}$ and $\Lambda_{vv,z}$ is expected, where the length scales are constant away from the boundaries and go to zero as the inner and outer radii are approached. The two scales are approximately equal in the central region where $\Lambda_{uu,z} = .082R_o$ and $\Lambda_{vv,z} = .090\ R_o$. The relative behavior of $\Lambda_{uu,z}$ and $\Lambda_{vv,z}$ as the boundaries are approached is consistent with recent theoretical work by Lewellen and Sandri (Ref. 14). $\Lambda_{uu,z}$ decreases more rapidly than $\Lambda_{vv,z}$ near the walls because the normal velocity (u) is affected more readily by the presence of a wall than the parallel velocity (v). Such behavior is the cornerstone of the Lewellen-Sandri model.

The behavior of $\Lambda_{ww,z}$ is more complex than for the other two scales. We first note that $\Lambda_{ww,z} \sim 3\Lambda_{uu,z}$ and this is a common feature of turbulent shear flows. The length scale in the downstream direction for the velocity receiving energy by direct production will be the largest scale in the field and is typically 2 to 8 times the various other length scales. The decrease in $\Lambda_{ww,z}$ near $r = .43$ is associated with the zero mean gradient and a similar behavior was observed by Sabot and Comte-Bellot in pipe flow. Results from their work are presented in Figure 10, and $\Lambda_{ww,z}$ is a minimum at $r = 0$ where $dW/dr = 0$. The values for $\Lambda_{uu,z}$ are also shown and agree with those observed in the present study. The values of $\Lambda_{ww,z}$ given by Sabot and Comte-Bellot are much greater than those obtained here and Hassan et.al.; data from Hassan et.al. is

---

13. Hassan, H. A., Jones, B. G. and Adrian, R. J., "Measurements and Axisymmetric Model of Spatial Correlations in Turbulent Pipe Flow," AIAA Report No. 79-1562, 1979.

14. Lewellen, W. S. and Sandri, G., "Incorporation of an Anisotropic Scale into Second-Order Closure Modeling of the Reynold Stress Equation," A.R.A.P. Tech Memo No. 80-11 (Submitted to J. Fluid Mech., 1980).

also included in Figure 10. (We have carefully reviewed other works by Sabot and Comte-Bellot, and they consistently report values of $\Lambda_{ww,z}$ greater than observed by other workers.) The increase in $\Lambda_{ww,r}$ near $r = .85$ in the present data may be related to the general parabolic behavior of $\Lambda_{ww,z}$ in pipe flow. Precise agreement between pipe and annulus flow is not expected, but the behavior of $\Lambda_{ww,z}$ in the present study is consistent with pipe flow data.

We compare the $\Lambda_{ww,z}$ data with the von Karman length scale, Λ_{VK}, defined as follows for plane parallel flow,

$$\Lambda_{VK} = \frac{dW/dy}{d^2W/dy^2}$$

where y is the cross-stream gradient direction. The motivation for this definition is that away from flow boundaries, the scale will be determined by local derivatives of W, and a rational choice is the first and second derivatives. An analogous expression for Λ_{VK} in cylindrical coordinates is

$$\Lambda_{VK} = \frac{dW/dr}{(1/r)(d/dr)(rdW/dr)}$$

Λ_{VK} was computed using our mean velocity field and the results are presented in Figure 11. The von Karman length possesses a number of features which are consistent with the $\Lambda_{ww,z}$ data, although these features tend to be exaggerated. The general level of Λ_{VK} is of the same order as $\Lambda_{ww,z}$, Λ_{VK} is greater near the outer wall than near the inner wall, and Λ_{VK} is small in the region of small mean gradient. It is remarkable that given the simplicity of the von Karman scale, it behaves as similarly to the data as observed.

The autocorrelation results can be compared to concepts derived for isotropic and homogeneous turbulence, and although the annulus flow is neither isotropic nor homogeneous, the data do have certain features in common with such flows. The correlation tensor may be completely specified by two scalar functions f and g, for isotropic, homogeneous turbulence, and these functions are dependent only on the magnitude of the separation vector. This is discussed in The Theory of Homogeneous Turbulence by Batchelor, (Ref.15) and Figure 12 is used to define the f and g functions. A separation vector, $\underline{r}$, is specified and velocities parallel and normal to $\underline{r}$ are defined as u_p and u_n, respectively. The following definitions are taken:

$$\overline{u_p(\underline{x})\, u_p(\underline{x} + \underline{r})} \equiv u^2 f(r)$$

$$u_n(\underline{x})\, u_n(\underline{x} + \underline{r}) \equiv u^2 g(r)$$

---

15. Batchelor, G. K., The Theory of Homogeneous Turbulence, Cambridge University Press, 1967.

where

$$u_n^2 = u_p^2 = u^2$$

by isotropy. The functions f and g depend only on the magnitude of $\underline{r}$ and for incompressible flows, the following constraint exists,

$$g = f + (r/2)(\partial f/\partial r)$$

The behavior of f and g is such that $f(0) = g(0) = 1$, f will have a long positive tail for large r, and g will go through zero or become negative for relatively small r.

The data is now placed in the context of f and g functions. The separation direction is Δz, so that w plays the role of the parallel velocity, while both u and v play the role of the perpendicular velocity. Autocorrelation data from $r = .75$ is presented in Figure 13 for the three velocity components and the autocorrelation lag time, τ, is related to Δz by $W\tau = \Delta z$. Both R_{uu} and R_{vv} behave g-like, becoming zero at $\Delta z/R_0 \simeq .3$, while R_{ww} is f-like, remaining positive for separations greater than $1.2R_0$. A more sensitive test to isotropic concepts involves the length scales Λ_f and Λ_g, defined by

$$\Lambda_f = \int_0^\infty f\,dr$$

$$\Lambda_g = \int_0^\infty g\,dr$$

and the constraint, $g = f + (r/2)(\partial f/\partial r)$, yields

$$\Lambda_g/\Lambda_f = 0.5$$

The following correspondences are made,

$$\Lambda_g \rightarrow \tilde{\Lambda}_{uu,z}\ ,\ \tilde{\Lambda}_{vv,z}$$

$$\Lambda_f \rightarrow \tilde{\Lambda}_{ww,z}$$

and the ratios $\tilde{\Lambda}_{uu,z}/\tilde{\Lambda}_{ww,z}$ and $\tilde{\Lambda}_{vv,z}/\tilde{\Lambda}_{ww,z}$ are tabulated below for three radial positions, $r = .27$, $.43$, and $.75$ where all lengths are nomalized by R_0. (The tilda is placed over Λ to emphasize that these scales were obtained by integrating the correlation functions out beyond τ_0).

	$\tilde{\Lambda}_{uu,z}/\tilde{\Lambda}_{ww,z}$	$\tilde{\Lambda}_{vv,z}/\tilde{\Lambda}_{ww,z}$
r = .27	.22	.26
r = .43	.26	.30
r = .75	.20	.22

All ratios are well below the 0.5 value associated with isotropic flow. The ratio of $\tilde{\Lambda}_{vv,z}/\tilde{\Lambda}_{ww,z}$ at r = .43 is the closest to 0.5 because the flow is nearly isotropic locally, no local production of w occurs, and the v velocity is not as sensitive to boundaries as u. It is not surprising that the above ratios differ substantially from 0.5 because of the use of $\tilde{\Lambda}_{ww,z}$. The w velocity receives energy by direct production, and quantities related to w are not expected to satisfy isotropic relations. In the following section, two-point measurements give a separation in the radial direction and the correlation functions for u and v are f and g-like, respectively. Results for that case will be in closer agreement with isotropic concepts and the data in the present section is given for future comparison with the two-point data.

VI. TURBULENT LENGTH SCALES VIA TWO-POINT CORRELATIONS

Two-point correlations for u, v and w, and two-point cross-correlations for u and w were measured for the case of pure radial separations. Three fixed probe positions were chosen, $r_F = .27$, .43, and .75, where the mean velocity gradient was positive, zero, and negative, respectively. Such measurements allowed an examination of the effects of mean shear and boundaries on the correlation functions. Data from the two-point correlation measurements are presented in Figures 14, 15, and 16 for the three fixed probe positions; the notation is one in which curves labeled u refer to R_{uu}, defined as

$$\overline{u^2}\, R_{uu}(r_F;\, \Delta r) \equiv \lim_{T\to\infty} \frac{1}{2T} \int_{-T}^{+T} u(r_F,t)\, u(r_F + \Delta r,t)\, dt$$

The curves labeled v and w refer to R_{vv} and R_{ww} which are defined similarly.

Data from $r_F = .27$, where dW/dr is positive, are presented in Figure 14. In the region between the inner tube ($R_I = .118$) and r_F, $R_{ww} > R_{uu} > R_{vv}$, and R_{vv} is negative for $r \lesssim .18$. The region outward from r_F shows a similar behavior, $R_{ww} > R_{uu} > R_{vv}$ out to $r \simeq .38$; beyond that point, R_{uu} and R_{vv} possess long positive tails and R_{ww} goes negative. Data from the zero mean gradient position, $r_F = .43$, are shown in Figure 15, and the following relationships hold for all separations, $R_{uu} > R_{ww} > R_{vv}$. This result differs from the previous case (and, as will be seen, from the $r_F = .75$ case) and is related to the zero mean gradient. Figure 16 shows data from $r_F = .75$ where dW/dr was negative. In the region approaching the outer wall ($.75 < r < 1.0$), $R_{ww} > R_{uu} > R_{vv}$, and R_{vv} goes negative for $r \gtrsim .87$. This behavior is similar to that observed in the $r_F = .27$ case for the region between the inner tube, and r_F. This similarity results from the fact that both regions possess relatively constant shear and are near boundaries. The results for $r < .75$ show $R_{ww} > R_{uu}$ until $r \simeq .55$, $R_{uu} \gg R_{ww}$ for $r \lesssim .55$. R_{uu} possesses a long positive tail, and this is similar to the behavior in the $r_F = .27$ case. In both instances, R_{uu} remains positive and decays slowly as one moves away from the near boundary. Both R_{ww} and R_{vv} go negative for $r < .75$, but R_{vv} becomes negative for much smaller separations than does R_{ww}.

Cross-correlations for u and w were measured and defined as

$$\left(\overline{u^2}\right)^{1/2}\left(\overline{w^2}\right)^{1/2} R_{uw}(r;\Delta r) \equiv \lim_{T\to\infty} \frac{1}{2T} \int_{-T}^{+T} u(r,t)\, w(r + \Delta r,t)\, dt$$

and

$$\left(\overline{u^2}\right)^{1/2}\left(\overline{w^2}\right)^{1/2} R_{wu}(r;\Delta r) \equiv \lim_{T\to\infty} \frac{1}{2T} \int_{-T}^{+T} w(r,t)\, u(r + \Delta r,t)\, dt$$

We note that for $\Delta r = 0$,

$$R_{uw}(r;0) = R_{wu}(r;0) = \text{Shear Stress Coefficient}$$

while for $\Delta r \neq 0$, R_{uw} and R_{wu} need not be equal. Data from the three fixed probe positions, $r_F = .27$, .43 and .75 are presented in Figure (17), (18) and (19), respectively. The cross correlations at $r_F = .27$ behave such that $R_{uw} \simeq R_{wu}$ in the region between the inner tube and r_F, where the mean velocity gradient is fairly constant, while for $r > r_F$, $R_{wu} > R_{uw}$ in a region where the mean gradient is rapidly decreasing. Figure (18) shows data taken about the zero gradient position, $r = .43$, and we find that $|R_{uw}| > |R_{wu}|$ for all radial separations. We note that $R_{uw}(\Delta r = 0) = R_{wu}(\Delta r) \neq 0$ because the fixed probe was not precisely at the zero mean gradient position. It is most likely that $R_{wu}(\Delta r)$ would have been zero for all separations if the fixed probe had been positioned at the precise zero stress point. The sign of R_{uw} is consistent with the sign of the turbulent stress $R_{uw}(r;\Delta r = 0)$ and $|R_{uw}|$ reaches a maximum value of approximately .18 for separations, Δr, of about .14. The $r_F = .75$ case is presented in Figure (19), and the results are very similar to those at $r_F = .27$. $R_{uw} \simeq R_{wu}$ in the region approaching the other wall $(.75 < r < 1.0)$ where the mean velocity gradient is approximately constant. In the region where the mean gradient is rapidly changing, $r < .75$, $R_{wu} > R_{uw}$, and this is similar to the behavior observed at $r_F = .27$.

The correlation functions described above were integrated along Δr to obtain turbulent length scales in the following manner,

$$\Lambda_{uu,r} \equiv \int_0^{\Delta r_0} R_{uu}(r_F; \Delta r)\, d(\Delta r)$$

The notation is the same as discussed in Section 5 and Δr_0 is the position at which R_{ab} becomes zero. The various length scales are tabulated in Table I, where the results from Section 5 are also included. Separations of plus and minus Δr were measured and integral scales for both cases are tabulated and denoted by the + and - signs. All lengths are normalized by R_0, and the negative values for $\Lambda_{uw,r}$ and $\Lambda_{wu,r}$ reflect the negative value for the corresponding correlation functions.

The tabulated length scales can be compared to pipe flow results obtained by Hassan et. al., Sabot, Renault and Comte-Bellot (Ref. 16), and Sabot and Comte-Bellot. In all three papers, a complete map of R_{uu}, R_{ww}, R_{uw}, and R_{wu} was obtained for arbitrary values of Δr and Δz, and such data allow the computation of isocorrelation curves for the various tensor components. Hassan et. al. tabulate various length scales at $r_F = .65R_0$ (or $.35R_c$ from the pipe wall), while Sabot et.al. provide isocorrelation curves at $r = .50R_0$, but do not tabulate the various length scales. Data from the present work, Hassan et. al. and Sabot et. al. are tabulated in Table II.

16. Sabot, J., Renault, J. and Comte-Bellot, G., "Space-Time Correlations of the Transverse Velocity Fluctuation in Pipe Flow," Phys. Fluids 16, No. 9, 1973, pp. 1403-05.

TABLE I

r_F		$\Lambda_{uu,r}$	$\Lambda_{vv,r}$	$\Lambda_{ww,r}$	$\Lambda_{uw,r}$	$\Lambda_{wu,r}$	$\Lambda_{uu,z}$	$\Lambda_{vv,z}$	$\Lambda_{ww,z}$
.27	+	.089	.064	.076	-.026	-.077	.068	.088	.240
	-	.049	.037	.061	-.038	-.033			
.43	+	.110	.065	.078	~ 0	~ 0	.082	.090	.196
	-	.082	.058	.064					
.75	+	.069	.048	.090	.048	.046	.082	.090	.242
	-	.093	.050	.100	.051	.079			

Table II

	$\Lambda_{ww,r}$	$\Lambda_{uu,r}$	$\Lambda_{uw,r}$	$\Lambda_{ww,r}$	$\Lambda_{ww,z}$	$\Lambda_{uu,z}$
Present $r = .75R_o$	.100	.093	.051	.079	.242	.082
Hassan et.al. $r = .65R_o$	.134	.083	.057	.051	.587	.083
Sabot et.al. $r = .50R_o$			$\sim .068$	$\sim .110$	1.000	.130

All separations in direction away from pipe wall

All lengths are divided by R_o and are derived from correlations with a radial separation away from the wall. Sabot et.al. gave values for $\Lambda_{ww,z}$ and $\Lambda_{uu,z}$, while $\Lambda_{uw,r}$ and $\Lambda_{wu,r}$ were obtained by reading the respective isocorrelation curves, plotting the data, and integrating the correlation curve. This is not a very accurate technique and we note this by use of the approximation symbols. A comparison between the present results and Hassan's shows that $\Lambda_{uu,r}$, $\Lambda_{uu,z}$, and $\Lambda_{uw,r}$ all agree to within approximately 10%, while $\Lambda_{ww,r}$ differs by about 30%. Inspection of Sabot's results shows that all their length scales are greater than observed here, or by Hassan and this was discussed in Section 5. The difference in $\Lambda_{ww,z}$ observed by Sabot et.al. and Hassan et.al. is disturbing, as both measurements were made at downstream distances of 90 diameters, which insures well developed flow. The relatively low value obtained here may be a consequence of the different geometry (annulus versus pipe) and the lack of a fully developed flow field. We can look to the work of Laufer for a third value of $\Lambda_{ww,z}$ to compare with Sabot's and Hassan's values. Laufer does not give $\Lambda_{ww,z}$ values directly and one must interpret the given power spectra and estimate $\Lambda_{ww,z}$; this was done and the values obtained from Laufer support the $\Lambda_{ww,z} \sim 0.6R_o$ value of Hassan.

Substantial differences exist for the behavior of the cross-correlation functions, R_{uw} and R_{wu}, for the three sets of data (Sabot, Hassan, and present). Both Sabot et.al. and we found $|R_{wu}| > |R_{uw}|$ for pure radial separations away from the outer wall, and we will subsequently show that such behavior is consistent with the production terms in the cross-correlation equations. Hassan et.al. found that $|R_{uw}| \gtrsim |R_{wu}|$ for pure radial separations, and the difference between Sabot et.al. and Hassan et.al. is again perplexing, given the similarity of their experiments.

We end this discussion by noting that a number of differences exist in the literature regarding turbulent pipe flow. In Section 4, the question of isotropy at pipe center was raised and a careful reading of Laufer, Hassan

et.al., and Sabot et.al. shows comparable discrepancies between the ratio u/w at similar radial positions. Differences in the various turbulent length scales exist (most notably in $\Lambda_{ww,z}$) and differences in the structure of the correlation functions (the behavior of R_{uw} and R_{wu}) are also observed. This state of affairs complicates the work of turbulent modelers. The correct modeling of the "tendency to isotropy" term in 2nd order closure schemes is very important and requires good, consistent data on the relative behavior of u, v, and w. As turbulent modeling becomes more sophisticated and length scale structure is introduced, high quality, consistent data on the various turbulent scales will be required. It is for these reasons that the discrepancies between the various pipe flow experiments are very disturbing.

The two-point, radial separation data can be interpreted using isotropic and homogeneous turbulence concepts in a manner similar to that discussed in Section 5. The separation direction was radial so that u plays the role of the parallel velocity, while v and w play the role of the transverse, or normal, velocity. It will be shown that the w correlations are g-like only at the zero mean gradient position where no direct production of w is occuring. The data from $r_F = .27$ show that $R_{uu} > R_{vv}$ in accord with the f and g-like character of isotropic turbulence. For $R_I < r < .27$ R_{vv} has a negative region, while R_{vv} remains positive for $r > .27$. The behavior of R_{ww} is not consistent with isotropic concepts as $R_{ww} > R_{uu}$ for $R_0 < r < .48$, and this is a consequence of the direct production of w by the mean gradient. The correlation functions at the zero gradient position, $r_F = .43$, behave in a manner expected from isotropic theory. The R_{uu} correlation is f-like and is always greater than R_{vv} and R_{ww}, while both R_{vv} and R_{ww} have negative regions in a g-like manner. At $r_F = .75$, $R_{uu} > R_{vv}$ and the two correlation functions behave f and g-like, respectively. Again, R_{ww} is not g-like because the non-zero mean gradient results in direct production of w.

The f and g length scales can be defined by the correspondence,

$$\Lambda_f \rightarrow \tilde{\Lambda}_{uu,r}$$

$$\Lambda_g \rightarrow \tilde{\Lambda}_{vv,r} \cdot \tilde{\Lambda}_{ww,r}$$

where the tilda again is used to emphasize that these length scales are obtained by integrating beyond Δr_0. The following ratios, $\tilde{\Lambda}_{vv,r}/\tilde{\Lambda}_{uu,r}$ and $\tilde{\Lambda}_{ww,r}/\tilde{\Lambda}_{uu,r}$, are tabulated below for the three fixed probe positions, and we distinguish between positive and negative Δr by + and -.

		$\tilde{\Lambda}_{vv,r}/\tilde{\Lambda}_{uu,r}$	$\tilde{\Lambda}_{ww,r}/\tilde{\Lambda}_{uu,r}$
	+	.72	.70
r_F = .27	-	.67	.79
	+	.53	.69
.43	-	.70	.70
	+	.58	1.30
.75	-	.47	.90

The values here are much closer to the ~0.5 value than observed in Section 5, and this is a consequence of using $\Lambda_{uu,r}$, which is derived from a velocity component not receiving energy by direct production. The values closest to 0.5, occur at r_F = .43 where the mean gradient is zero, and for positive separations, which are in the direction of the far wall and affected less by boundaries than the negative separation case.

The equations for the various correlation functions may be readily derived for the present flow configuration, and the derivation is presented in Appendix B. All the equations have a similar form, and we present the $\tilde{R}_{ww}(\underline{r};\Delta\underline{r})$ equation as a model,

$$\frac{\partial \tilde{R}_{ww}}{\partial t} + \tilde{A}_{ww} + \left[\tilde{R}_{uw}\left(\frac{\partial W}{\partial r}\right)_1 + \tilde{R}_{wu}\left(\frac{\partial W}{\partial r}\right)_2\right]$$

$$= \tilde{D}_{ww} + \tilde{P}_{ww} + \tilde{V}_{ww}$$

where the subscripts 1 and 2 refer the positions $\underline{r}$ and $\underline{r} + \Delta\underline{r}$, respectively. The tilda denotes the correlation functions have not been normalized by the rms velocities (see Section 2). The A_{ww} term represents the advection of $\tilde{R}_{ww}$ and is equal to

$$\tilde{A}_{ww} = \left(w\frac{\partial}{\partial z}\right)_1 \tilde{R}_{uu} + \left(\frac{W}{\partial z}\right)_2 \tilde{R}_{uu} \qquad 6\text{-}1$$

The bracketed term in Eq. (6-1) is the production term, and is the one on which we will concentrate. The $\tilde{D}_{ww}$ term represents turbulent diffusion and is comprised of third order velocity correlations, while the $\tilde{P}_{ww}$ term is the velocity-pressure gradient correlation and $\tilde{V}_{ww}$ represents the viscous diffusion term. The equations for the other non-zero tensor components are presented below where the various terms are analogous to those described above.

$$\frac{\partial \tilde{R}_{uu}}{\partial t} + \tilde{A}_{uu} = \tilde{D}_{uu} + \tilde{P}_{uu} + \tilde{V}_{uu} \qquad 6\text{-}2$$

$$\frac{\partial \tilde{R}_{vv}}{\partial t} + \tilde{A}_{vv} = \tilde{D}_{vv} + \tilde{P}_{vv} + \tilde{V}_{vv} \qquad 6\text{-}3$$

$$\frac{\partial \tilde{R}_{uw}}{\partial t} + \tilde{A}_{uw} + \tilde{R}_{uu}\left(\frac{\partial W}{\partial r}\right)_2 = \tilde{D}_{uw} + \tilde{P}_{uw} + \tilde{V}_{uw} \qquad 6\text{-}4$$

$$\frac{\partial \tilde{R}_{wu}}{\partial t} + \tilde{A}_{wu} + \tilde{R}_{uu}\left(\frac{\partial W}{\partial r}\right)_1 = \tilde{D}_{wu} + \tilde{P}_{wu} + \tilde{V}_{wu} \qquad 6\text{-}5$$

The equations for $\tilde{R}_{uu}$ and $\tilde{R}_{vv}$ do not have direct production terms, and the differences observed for these functions within the flow field are due to geometrical effects (boundaries) and the nature of the turbulent diffusion and velocity-pressure gradient terms (D_{ij} and P_{ij}). Equation (6-1) for R_{ww} shows a production term which provides a qualitative explanation of the $\Lambda_{ww,z}$ behavior. For the case of pure axial separation, $(\partial W/\partial r)_1 = (\partial W/\partial r)_2$, and at $r_F = .43$, the mean gradient is zero; this is consistent with the diminishing of $\Lambda_{ww,z}$ near the zero gradient position. The equations for R_{uw} and R_{wu} [Eqs. (6-4) and (6-5)] show production terms, $R_{uu}(\partial W/\partial r)_2$ and $R_{uu}(\partial W/\partial r)_1$, respectively. In regions of relatively constant mean gradient where $(\partial W/\partial r)_1 \approx (\partial W/\partial r)_2$, one can expect $R_{uw} \approx R_{wu}$, and this was found to be true. We write Eqs. (6-4) and (6-5) as follows,

$$\frac{\partial \tilde{R}_{uw}}{\partial t} = -\tilde{R}_{uu}\left(\frac{\partial W}{\partial r}\right)_1 + \begin{matrix}\text{Other}\\ \text{Terms}\end{matrix} \qquad 6\text{-}6$$

$$\frac{\partial \tilde{R}_{wu}}{\partial t} = -\tilde{R}_{uu}\left(\frac{\partial W}{\partial r}\right)_2 + \begin{matrix}\text{Other}\\ \text{Terms}\end{matrix} \qquad 6\text{-}7$$

and we inspect the behavior at $r_F = .43$, where $(\partial W/\partial r)_1 = 0$. The production term in Eq. (6-6) is then consistent with the behavior of R_{uw} being a relatively small quantity around $r_F = .43$. The production term, $-R_{uu}(\partial W/\partial r)_2 \neq 0$, in Eq. (6-7) is non zero as $(\partial W/\partial r)_2 \neq 0$ for separations about $r_F = .43$ and this agrees with the observed behavior, $|R_{wu}| > |R_{uw}|$. Also, the observed sign of R_{wu} is consistent with the production term in Eq. (6-7). Finally, we observe that the structure of the production terms for R_{uw} and R_{wu} will drive $|R_{wu}| > |R_{uw}|$ in the regions of rapidly changing shear, $r > r_F = .27$ and $r < r_F = .75$, as was observed.

VII. SUMMARY AND RECOMMENDATIONS

The present experimental study has provided a complete description of the mean and turbulent velocity fields in annular flow at a downstream distance of 30 diameters. A partial map of the correlation tensor components was also obtained as well as various turbulent length scales. A good deal of time and effort was devoted to upgrading the wind tunnel to research standards, and we are confident that the flow field is steady and symmetric to within such standards. The downstream position of 30 diameters was insufficient to provide fully developed flow as evidenced by the lack of isotropy at the zero mean gradient position. Even with this drawback, the velocity fields behaved as generally expected. The mean velocity followed a logarithmic profile, while the downstream fluctuations (w) behaved parabolically as a function of radius with the minimum occurring at the zero mean gradient position. The relative magnitudes of u and v were in line with previous shear flow results in the non-zero shear regions, where $w > v > u$. The behavior of the cross correlation coefficient was, again, in accord with previous pipe flow results, where $\overline{uw} / |u||w| \sim \pm .4$ in the regions of positive and negative mean gradients. The turbulent Reynolds stress was in approximate agreement with the theoretically derived expression and discrepancies between theory and experiment were probably due to a lack of fully developed flow.

The various turbulent length scales measured for the annulus flow were for the most part in accord with the results of other workers. Typically length scales for velocity correlations with pure radial separations were all of order one tenth the outer pipe radius. The behavior of $\Lambda_{uu,z}$ and $\Lambda_{vv,z}$ as a function of radius agreed with pipe flow results and their relative behavior near flow boundaries provided support for the two-scale turbulent models of Lewellen and Sandri. The $\Lambda_{ww,z}$ scale was a minimum at the zero mean gradient position. The magnitude of $\Lambda_{ww,z}$ was smaller than generally reported for pipe flow and this may be a consequence of the different geometry (annulus versus pipe) or the lack of fully developed flow. The length scale results were interpreted using a number of theoretical concepts. One was the von Karman length scale which is based on the ratio of local mean velocity derivatives. This simple model gave surprisingly good agreement with the general behavior of $\Lambda_{ww,z}$. The theoretical framework derived for isotropic turbulence was used to interpret certain length scale results. We found reasonable agreement between theory and experiment for length scales associated with the u and v velocities which do not receive energy by direct production. The best agreement occured for length scales measured about the zero mean gradient position where even w receives no energy by direct production. Finally, the full equations for the correlation functions were presented, and the production terms were examined; these terms were found to be consistent with our experimental results.

The present work has provided data on turbulent structure in annular flow. As previously stated, much effort was spent upgrading the facility to research standards, and we now have a research quality apparatus along with all the necessary data taking hardware and software. A number of research projects could now be undertaken for varying degrees of expense and we will outline them. The first project would be an exact repeat of the measurements described here at a downstream distance of 45 diameters (and possibly 15 diameters). This would provide data on the evolution of various flow quantities as a function of downstream distance. Such information would be of interest because not all flow variables come into equilibrium simultaneously. Certain variables obtain equilibrium markedly faster than others, such as the Reynolds stress coefficient. This was evidenced in our present results where the stress coefficient agreed with well developed pipe flow results, while u and v were still evolving (the lack of isotropy at the zero gradient position). Such a project would require no capital expenditures and could be done in approximately ½ man-year. A study which could be done with a small capital expenditure is a map of the various isocorrelations at positive, negative and zero mean gradient positions. This would require correlation measurements for simultaneous non-zero radial and axial separations, and a modification of probes and transversing mechanisms would be necessary. Such a study would provide a very complete determination of the effect of shear on turbulent structure, and would again require approximately ½ man-year.

The introduction of swirl to this flow field is still a goal of our research. Very little data exists on the behavior of swirling flows and given the large number of situations where swirl occurs, the importance of understanding such flows goes without saying. Two possibilities exist for the introduction of swirl in the present apparatus. One is to run the tunnel in its present configuration with the honeycomb and introduce swirl by use of vanes or "twisted tape". The efficiency of such a method would probably be low, so that high swirls could not be attained. The precise design of such a system would require trial and error, but should not be very expensive. Once swirl is introduced, one can measure the swirl decay rate as a function of downstream position, and this information would be extremely useful for comparison to the A.R.A.P. 2nd order turbulence model. Also, one can investigate the effect of swirl on the turbulent structure. Such effects would be analogous to stably stratified flow in the sense that both rotation and stratification can be stabilizing influences. The other way in which to introduce swirl is to go back to the original design concepts of this apparatus. The vanes situated at the inlet introduce swirl which is "spun-up" during the contraction process. It is precisely in the contraction section where we believe the asymmetries are introduced and modification of the contraction section is in order. The contraction section would be redesigned to provide a very smooth and uniform contraction for the purpose of eliminating any asymmetries. The advantage of such a technique is the generation of very high swirl levels, while the drawbacks involve the difficulty in creating symmetric flows in such a system and the fair amount of construction required. The rewards would be many because detailed characteristics of highly swirled flow could be studied and this would represent a true advance in our understanding of such flows.

APPENDIX A

The expression for the effective cooling velocity, U_c, of a hot wire or hot film sensor oriented at an angle α to the instantaneous velocity, U, is given below as

$$U_c = U\left[\cos^2\alpha + k^2 \sin^2\alpha\right]^{1/2} \tag{A.1}$$

where k is an experimentally determined quantity and the orientation of the flow and sensor are shown in Figure A-1(a). The output voltage, e, of an anemometer-linearizer system will be proportional to U, and we write

$$e = \gamma U_c \tag{A.2}$$

where γ is the calibration coefficient. The two sensors of the X-probe are labeled A and B, and are oriented at plus and minus 45^0 to the mean flow direction, $\bar{U}$, respectively. The output voltage for each sensor from an instantaneous velocity, U, oriented at an angle ϕ to the mean flow direction is given below as

$$e_A = \gamma\left[(\bar{U} + u')^2 + (v')^2\right]^{1/2}\left[\cos^2(\theta_A + \phi) + k^2 \sin^2(\theta_A + \phi)\right]^{1/2}$$

$$e_B = \gamma\left[(\bar{U} + u')^2 + (v')^2\right]^{1/2}\left[\cos^2(\theta_B + \phi) + k^2 \sin^2(\theta_B + \phi)\right]^{1/2}$$

The primed quantities are the fluctuating velocities and the orientation of sensor and velocity is shown in Figure A-1(b). The trigonometric functions are expanded and we make use of the fact that

$$\tan\phi = \frac{v'}{\bar{U} + u'} \approx \frac{v'}{\bar{U}} \ll 1$$

$$\tan\phi \approx \phi \approx \frac{v'}{\bar{U}}$$

this leads to the following expressions,

$$e_A = \frac{\gamma\bar{U}}{\sqrt{2}}\left[\left(1 + \frac{u'}{\bar{U}}\right)^2 + \left(\frac{v'}{\bar{U}}\right)^2\right]^{1/2}\left[(1 - 2\phi) + k^2(1 + 2\phi)\right]^{1/2} \qquad (A.3)$$

$$e_B = \frac{\gamma\bar{U}}{\sqrt{2}}\left[\left(1 + \frac{u'}{\bar{U}}\right)^2 + \left(\frac{v'}{\bar{U}}\right)^2\right]^{1/2}\left[(1 - 2\phi) + k^2(1 + 2\phi)\right]^{1/2} \qquad (A.4)$$

The above expressions may be further simplified by neglecting second order quantities and expanding the square root expressions (using $u'/\bar{U}$, $v'/\bar{U} \ll 1$, $\phi = v'/\bar{U}$).

$$e_A = \frac{\gamma\bar{U}}{\sqrt{2}}(1 + k^2)\left[1 + \frac{u'}{\bar{U}}\right]\left[1 - 2\left(\frac{1 - k^2}{1 + k^2}\right)\frac{v'}{\bar{U}}\right] \qquad (A.5)$$

$$e_B = \frac{\gamma\bar{U}}{\sqrt{2}}(1 + k^2)\left[1 + \frac{u'}{\bar{U}}\right]\left[1 - 2\left(\frac{1 - k^2}{1 + k^2}\right)\frac{v'}{\bar{U}}\right] \qquad (A.6)$$

The sum of e_A and e_B is taken as

$$e_S \equiv \frac{e_A + e_B}{2} = \frac{\gamma\bar{U}}{\sqrt{2}}(1 + k^2)\left(1 + \frac{u'}{\bar{U}}\right) \qquad (A.7)$$

and the average of e_S is

$$\overline{e_S} = \frac{\gamma\bar{U}}{\sqrt{2}}(1 + k^2) \equiv \frac{\gamma'\bar{U}}{\sqrt{2}} \qquad (A.8)$$

where γ' is the new calibration constant. The fluctuating voltage may be written as

$$e_S' = e_S - \bar{e}_S = \gamma' u'$$

and the difference of e_B and e_A is taken as

$$e_D \equiv \frac{e_B - e_A}{2} = \gamma' \bar{U} \left[1 + \frac{u'}{\bar{U}}\right] \left(\frac{1 - k^2}{1 + k^2}\right) \frac{v'}{\bar{U}} \qquad (A.9)$$

Second order terms are again neglected and we make use of the fact that $\bar{e}_D = 0$; this yields

$$e_D' = \gamma' \left(\frac{1 - k^2}{1 + k^2}\right) v' \qquad (A.10)$$

The apparent velocity fluctuations are defined in relation to the true fluctuations as follows,

$$u'_{apparent} = \frac{e_S'}{\gamma'} = u'_{true} \qquad (A.11)$$

$$v'_{apparent} = \frac{e_D'}{\gamma'} = \left(\frac{1 - k^2}{1 + k^2}\right) v'_{true} \qquad (A.12)$$

The above expression shows that the apparent transverse fluctuations must be corrected by the factor $(1+k^2/1-k^2)$ to yield the true value.

The k factor is determined experimentally by measuring the flow angle α and using Eq.(A.1). The measurement is a difficult one and a good deal of scatter exists for the k values determined here and by others (Jorgensen, 1971). The value of k depends on α, with the largest values of k occurring at $\alpha = 0$. At $\alpha = 45^0$, we find $k = .32 \pm .05$ for the hot film probes used in the present experiment, while Jorgensen (1971) found $k = .36 \pm .04$ for comparable hot film sensors. Friehe and Schwarz (1968) used a somewhat different expression for the effective cooling velocity than given in Eq.(A.1), and the correction factor they give is consistent with a value of $k = .28$ for hot film sensors.

APPENDIX B

The equations for the correlation tensor components can be derived for each component separately as follows, where the $\tilde{R}_{uw}$ component is chosen as an example. The following relationships are used:

$$\tilde{R}_{uw}(\underline{r};\Delta\underline{r}) = \overline{u(\underline{r})\, w(\underline{r}+\Delta\underline{r})} \qquad u_1 w_2$$

where

$$\underline{r} \rightarrow 1$$

$$\underline{r} + \Delta\underline{r} \rightarrow 2$$

and

$$\frac{\partial \tilde{R}_{uw}}{\partial t} = u_1 \frac{\partial w_2}{\partial t} + w_1 \frac{\partial u_1}{\partial t}$$

The preceeding definitions are used in conjunction with the Navier-Stokes equations for the turbulent fluctuations in cylindrical coordinates.

$$u_1 \left[\left(\frac{\partial w}{\partial t}\right)_2 + \left(u\frac{\partial w}{\partial r}\right)_2 + \left(u\frac{\partial w}{\partial r}\right)_2 + \left(\frac{v}{r}\frac{\partial w}{\partial \phi}\right)_2 + \left(w\frac{\partial w}{\partial z}\right)_2 + \left(w\frac{\partial w}{\partial z}\right)_2 = \right.$$

$$\left. - \left(\frac{\partial \pi}{\partial z}\right)_2 + \nu\left(\nabla^2 w\right)_2 \right]$$

$$w_2 \left[\left(\frac{\partial u}{\partial t}\right)_1 + \left(u\frac{\partial u}{\partial r}\right)_1 + \left(\frac{v}{r}\frac{\partial u}{\partial \phi}\right)_1 + \left(w\frac{\partial u}{\partial z}\right)_1 + \left(w\frac{\partial u}{\partial z}\right)_1 - \left(\frac{v^2}{r}\right)_2 = \right.$$

$$\left. - \left(\frac{\partial \pi}{\partial r}\right)_1 + \nu\left(\nabla^2 u - \frac{u}{r^2} - \frac{2}{r^2}\frac{\partial v}{\partial \phi}\right)_1 \right]$$

The above equations are averaged and added to yield

$$\frac{\partial \tilde{R}_{uw}}{\partial t} + \tilde{A}_{uw} + \overline{u_1 u_2}\left(\frac{\partial W}{\partial r}\right)_2 = \tilde{D}_{uw} + \tilde{P}_{uw} + \tilde{V}_{uw}$$

where the following definitions are used,

$$\tilde{A}_{uw} \equiv \left[W_1 \frac{\partial}{\partial z_1} + W_2 \frac{\partial}{\partial z_2} \right] R_{uw}$$

$$\tilde{D}_{uw} = -\left[\overline{u_1\left(u\frac{\partial w}{\partial r}\right)_2} + \overline{u_1\left(\frac{\partial v}{\partial r}\frac{\partial w}{\partial \phi}\right)_2} + \overline{u_1\left(w\frac{\partial w}{\partial z}\right)_2} + \overline{w_2\left(u\frac{\partial u}{\partial r}\right)_1} + \overline{w_2\left(\frac{v}{r}\frac{\partial u}{\partial \phi}\right)_1} + \overline{w_2\left(w\frac{\partial u}{\partial z}\right)_1} - \overline{w_2\left(\frac{v^2}{r}\right)_1} \right]$$

$$\tilde{P}_{uw} = -\left[\overline{u_1\left(\frac{\partial \pi}{\partial z}\right)_2} + \overline{w_2\left(\frac{\partial \pi}{\partial z}\right)_1} \right]$$

$$\tilde{V}_{uw} = \nu\left[\overline{u_1\left(\nabla^2 w\right)_2} + \overline{w_2\left(\nabla^2 u - \frac{u}{r} - \frac{2}{r}\frac{\partial v}{\partial \phi}\right)_1} \right]$$

The term $\tilde{A}_{uw}$ represents the advection of the correlation by the mean velocity while $\tilde{D}_{uw}$ represents turbulent diffusion and is comprised of third order correlations. P_{uw} represents the velocity pressure gradient correlations and V_{uw} is the viscous diffusion term. The equations for the other non-zero tensor components can be derived in a similar manner and are given in Section 6. We do not bother defining the $\tilde{A}$, $\tilde{D}$, $\tilde{P}$, and $\tilde{V}$ terms for all the correlation equations because they are never used and the example presented here shows the form of these terms. The production term is of interest and is presented in Section 6 for all the non-zero correlation components.

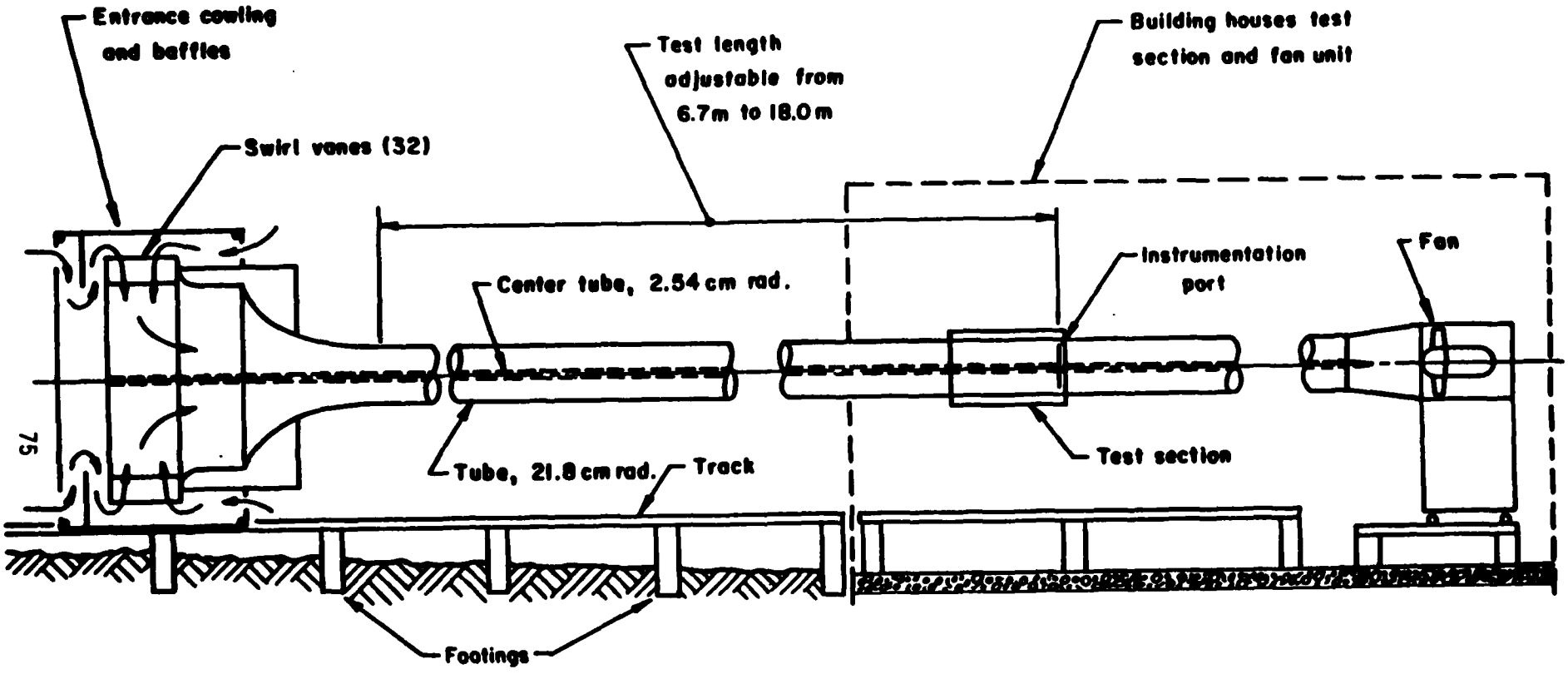

Figure 1 - Schematic of A.R.A.P. vortex tube tunnel.

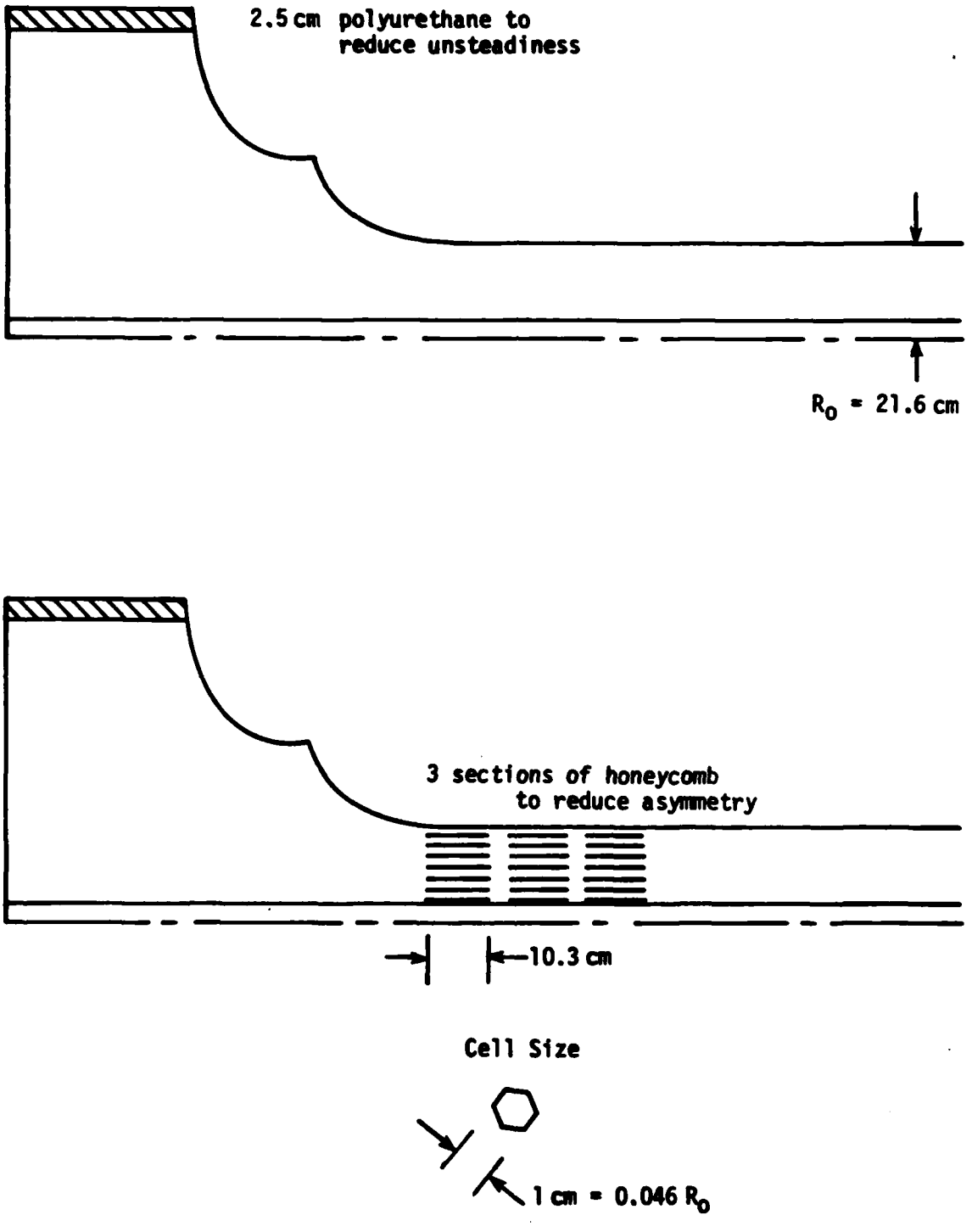

Figure 2 - Schematic of contraction section where the placement of the polyurethane and honeycomb sections is shown.

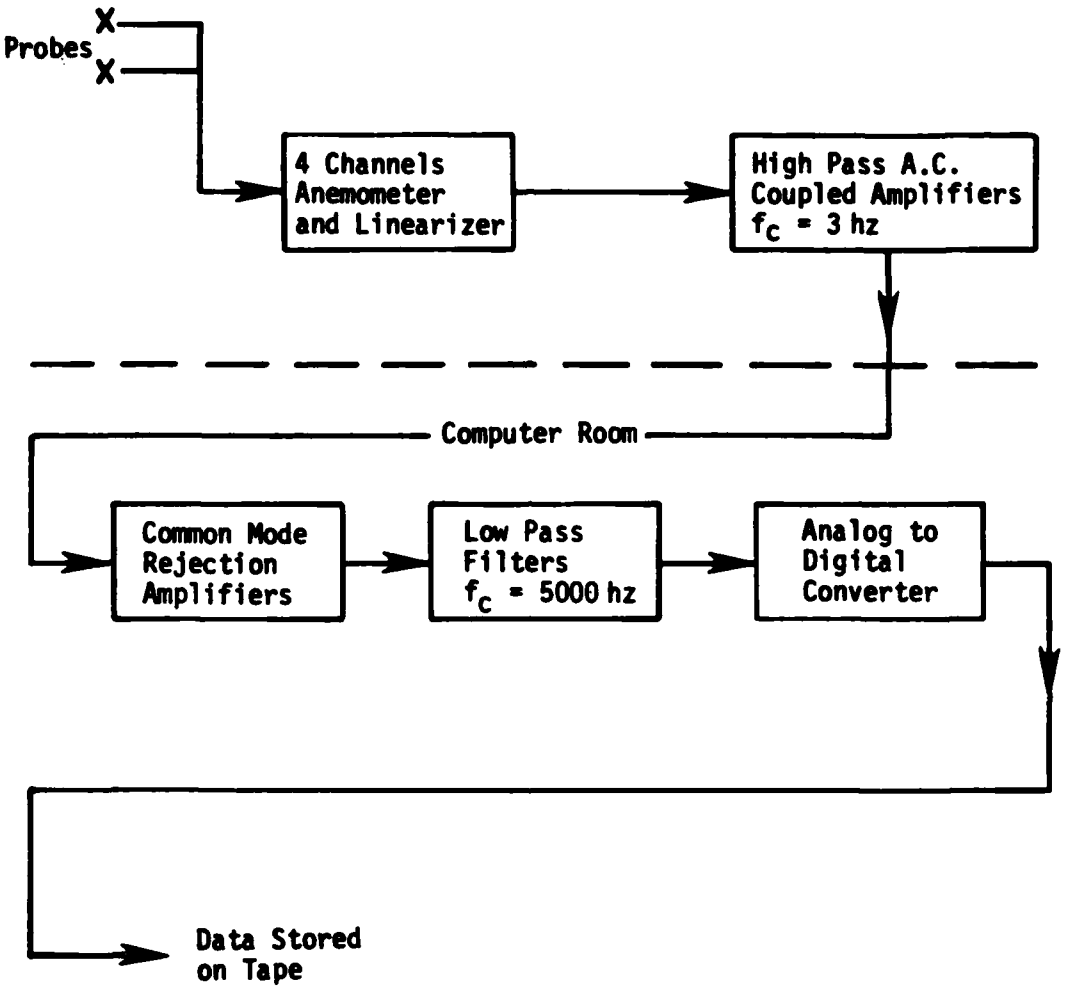

Figure 3 - Schematic of data acquisition system.

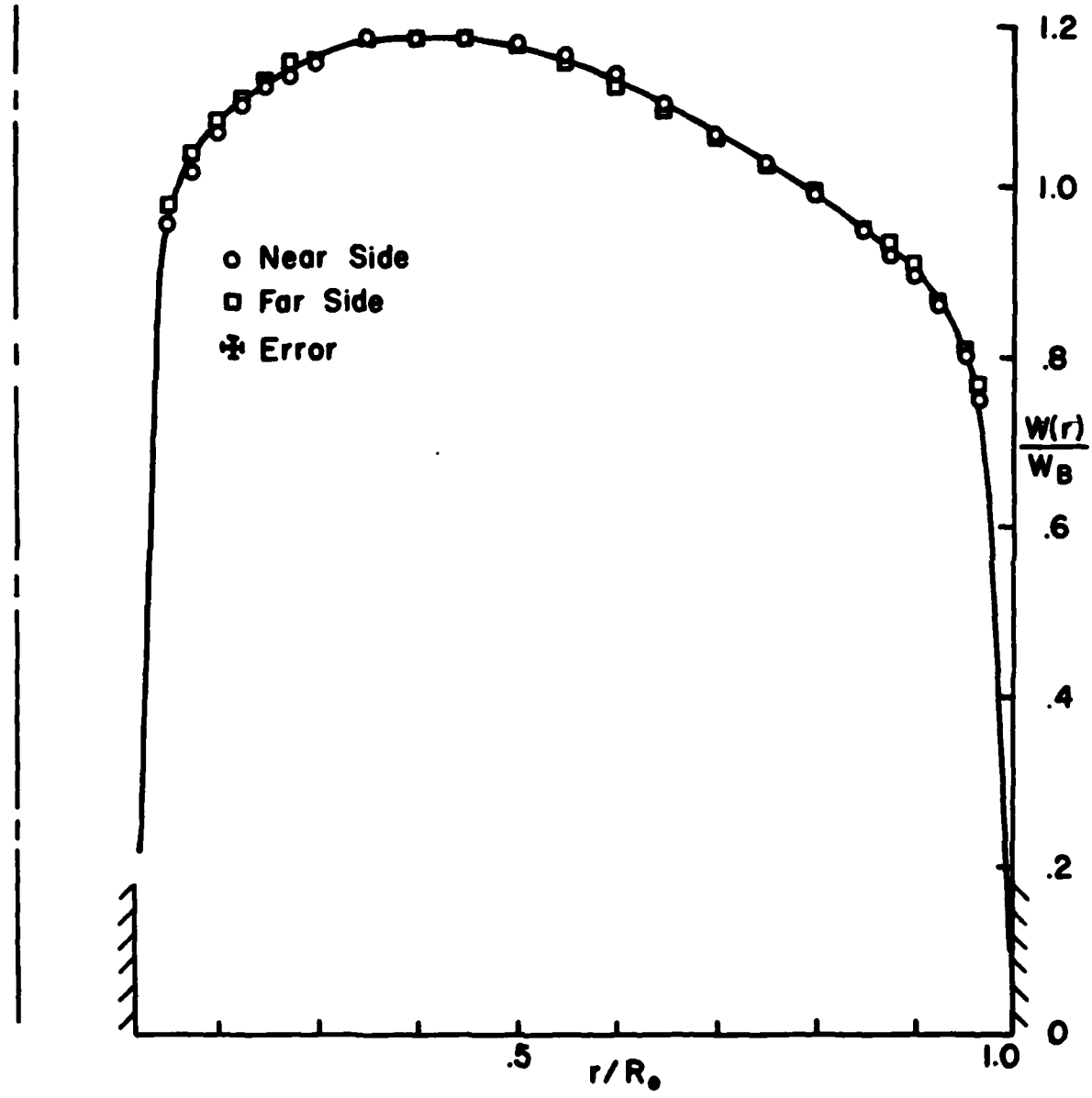

Figure 4 - Mean axial velocity vs. radial position.

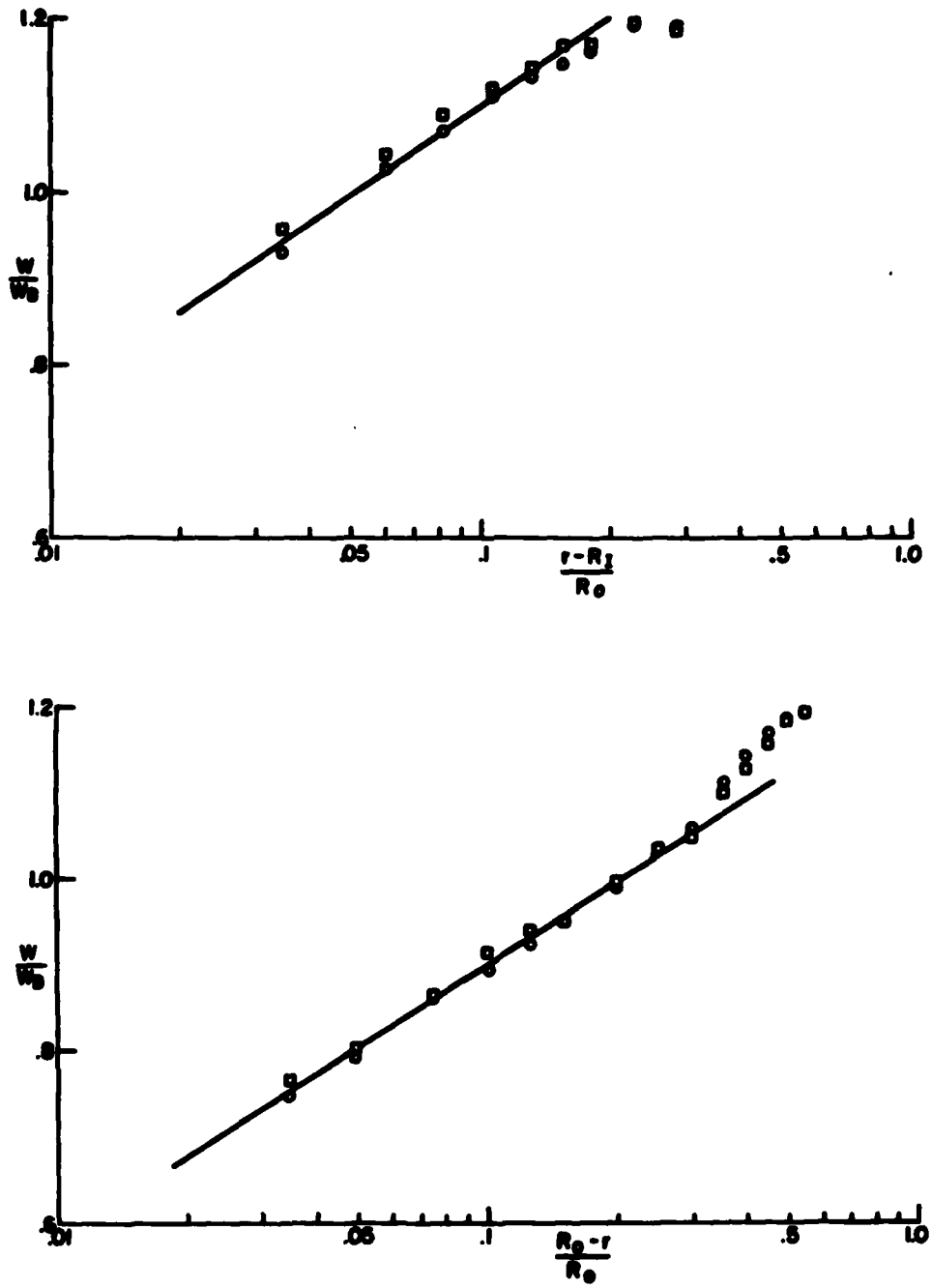

Figure 5 - Mean axial velocity vs. distance from wall: the upper and lower graphs are for distances away from the inner and outer walls, respectively.

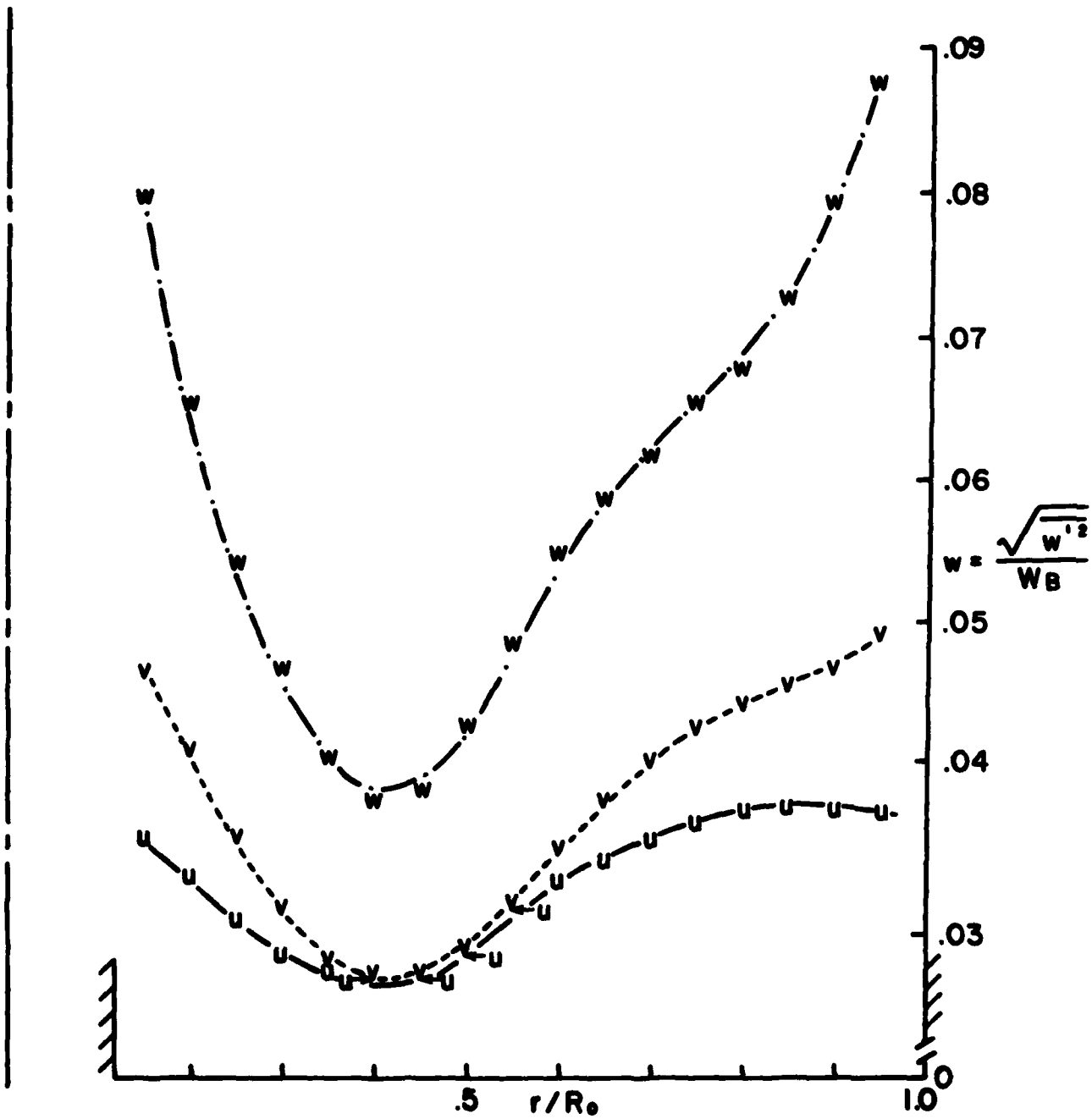

Figure 6 - Root mean square turbulent velocities vs. radial position.

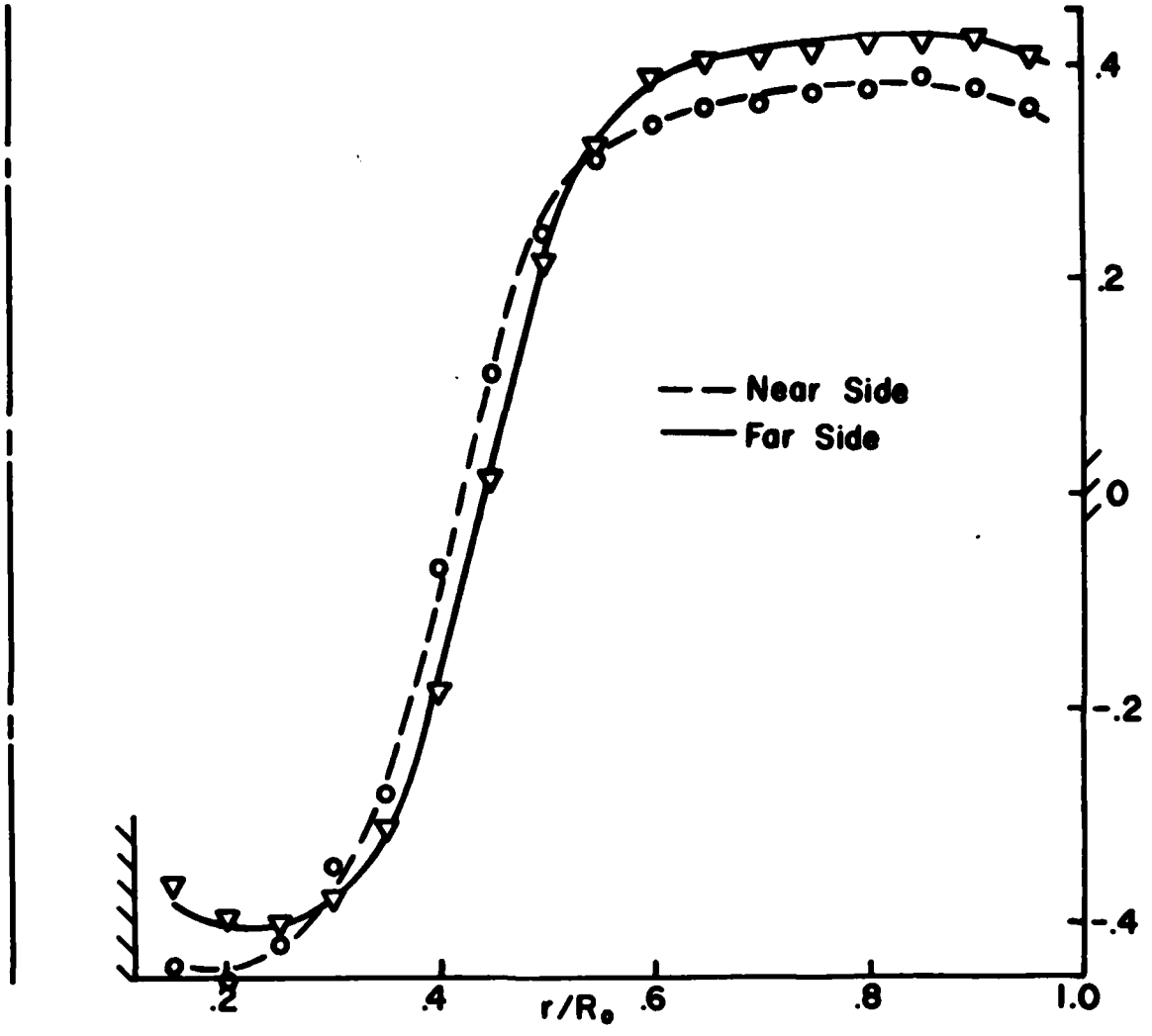

Figure 7 - Turbulent shear stress coefficient vs. radial position.

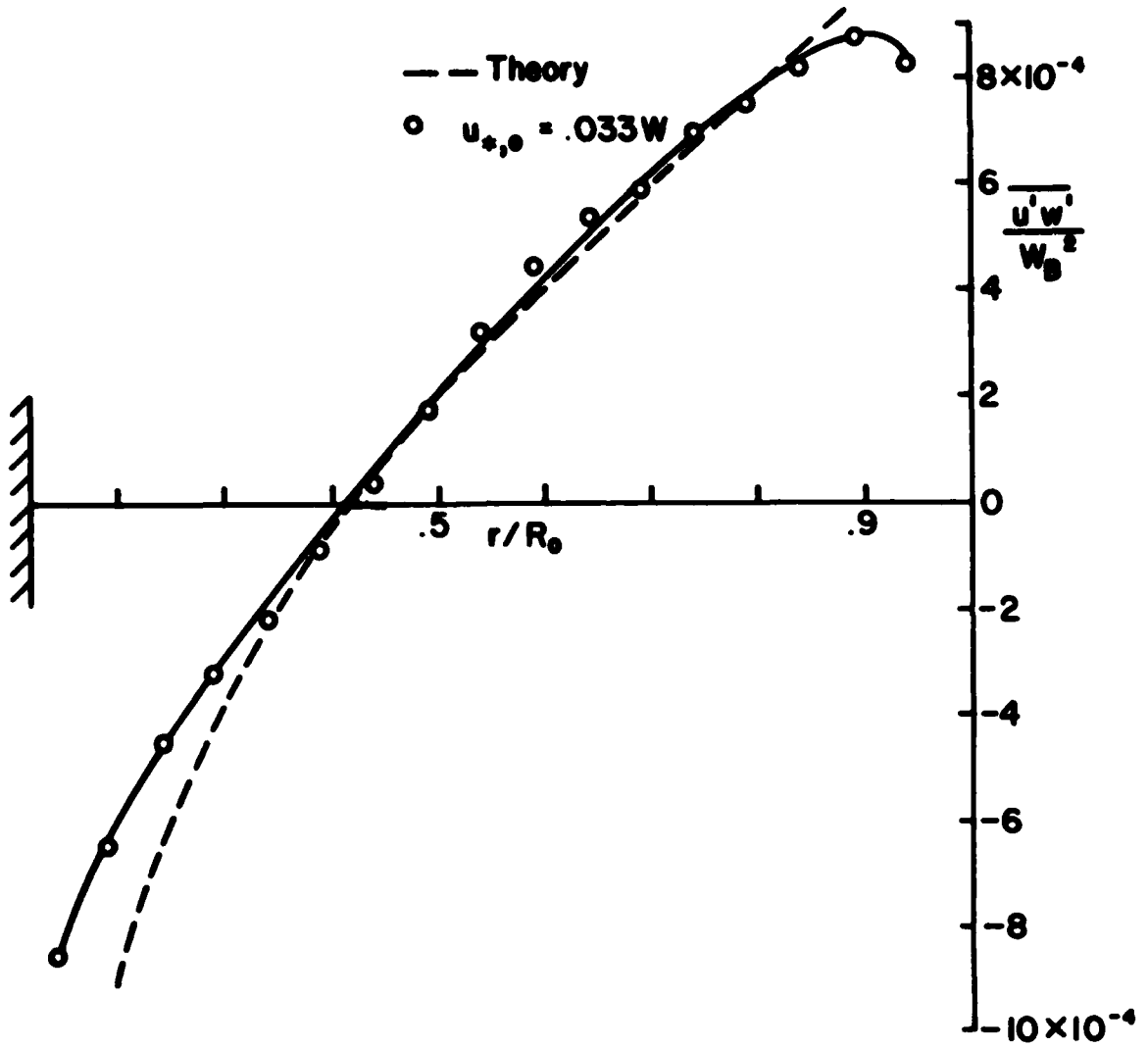

Figure 8 - Turbulent shear stress vs. radial position.

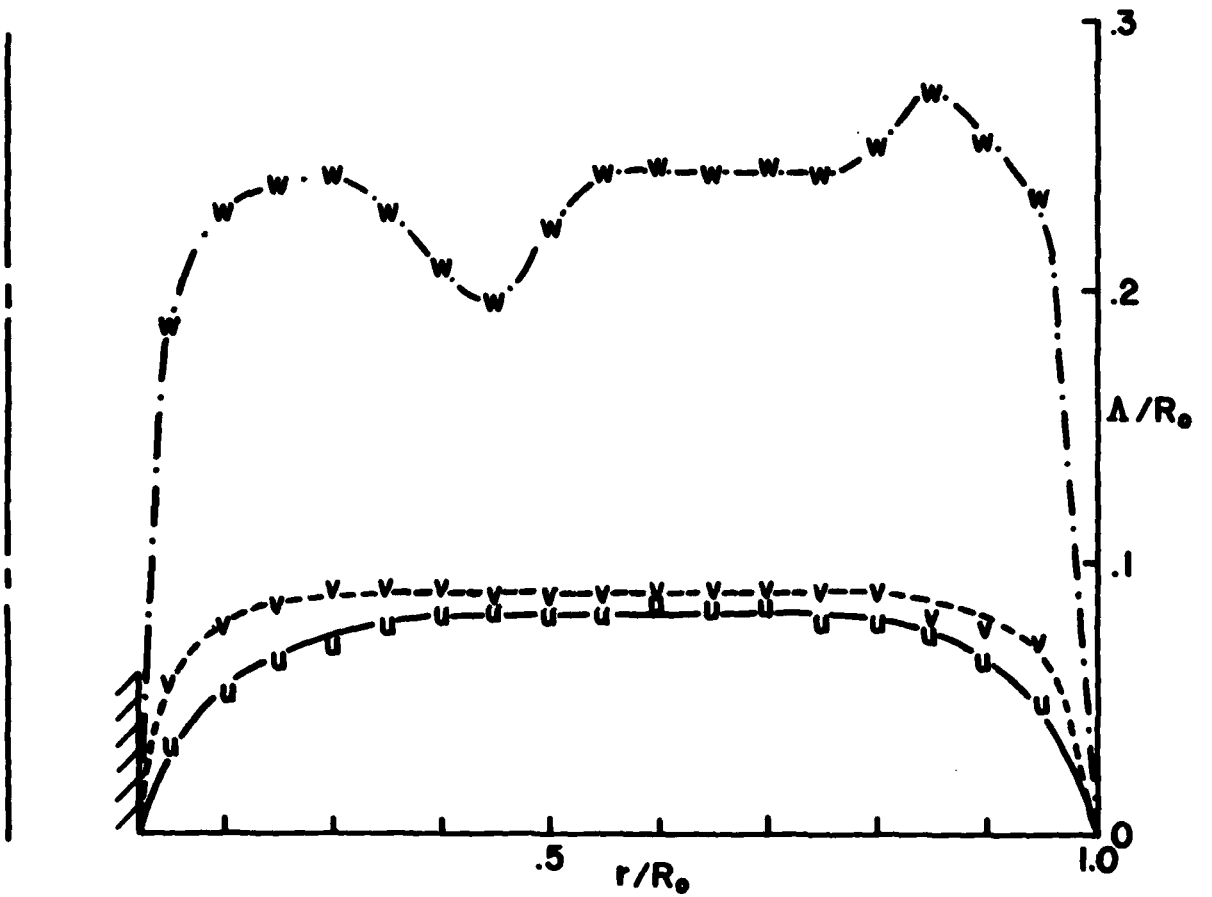

Figure 9 - Turbulent length scales vs. radial position.

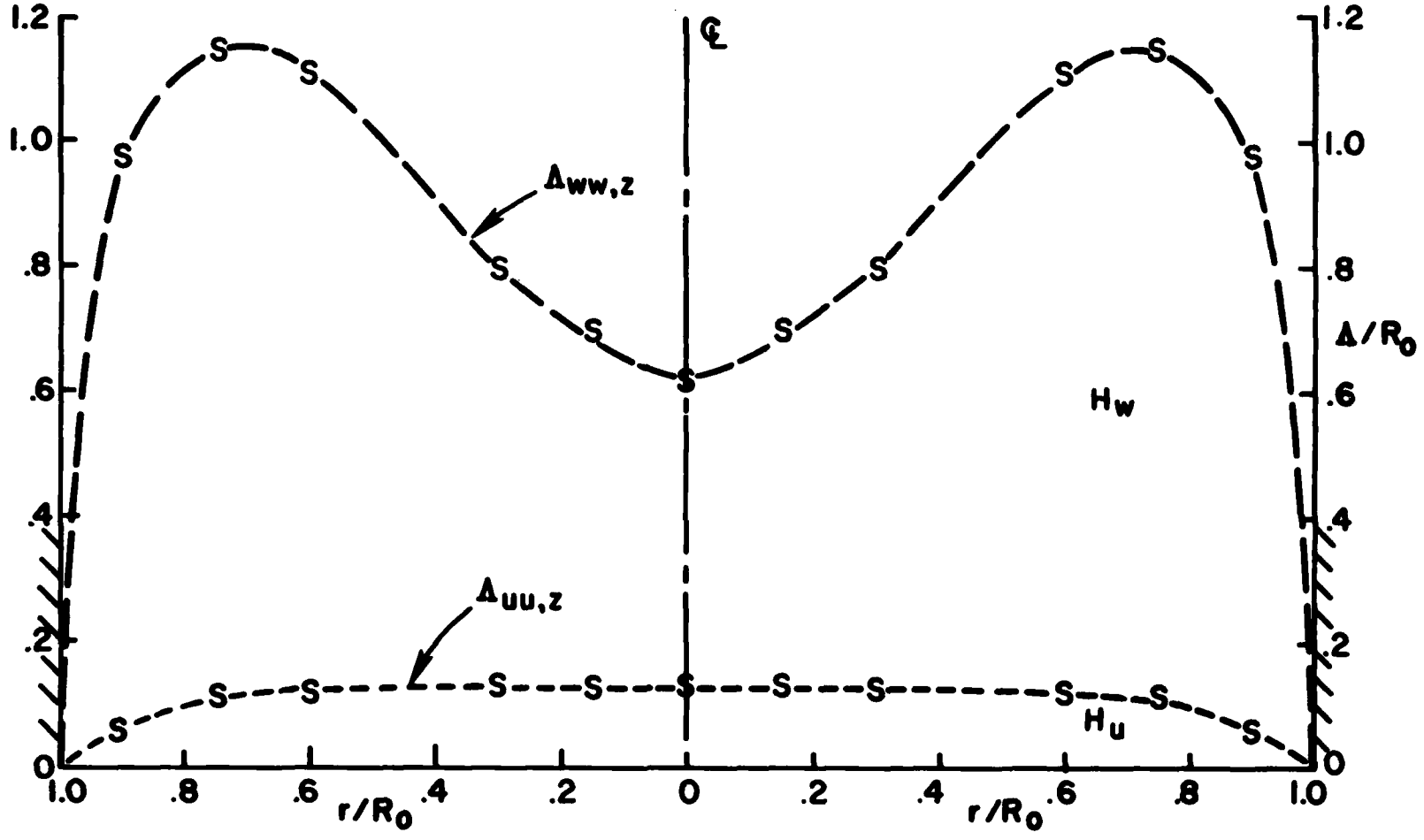

Figure 10 - Turbulent length scales vs. radial position constructed for data of Sabot and Comte-Bellot (Ref. 8) and Hassan, et.al. (Ref. 13).

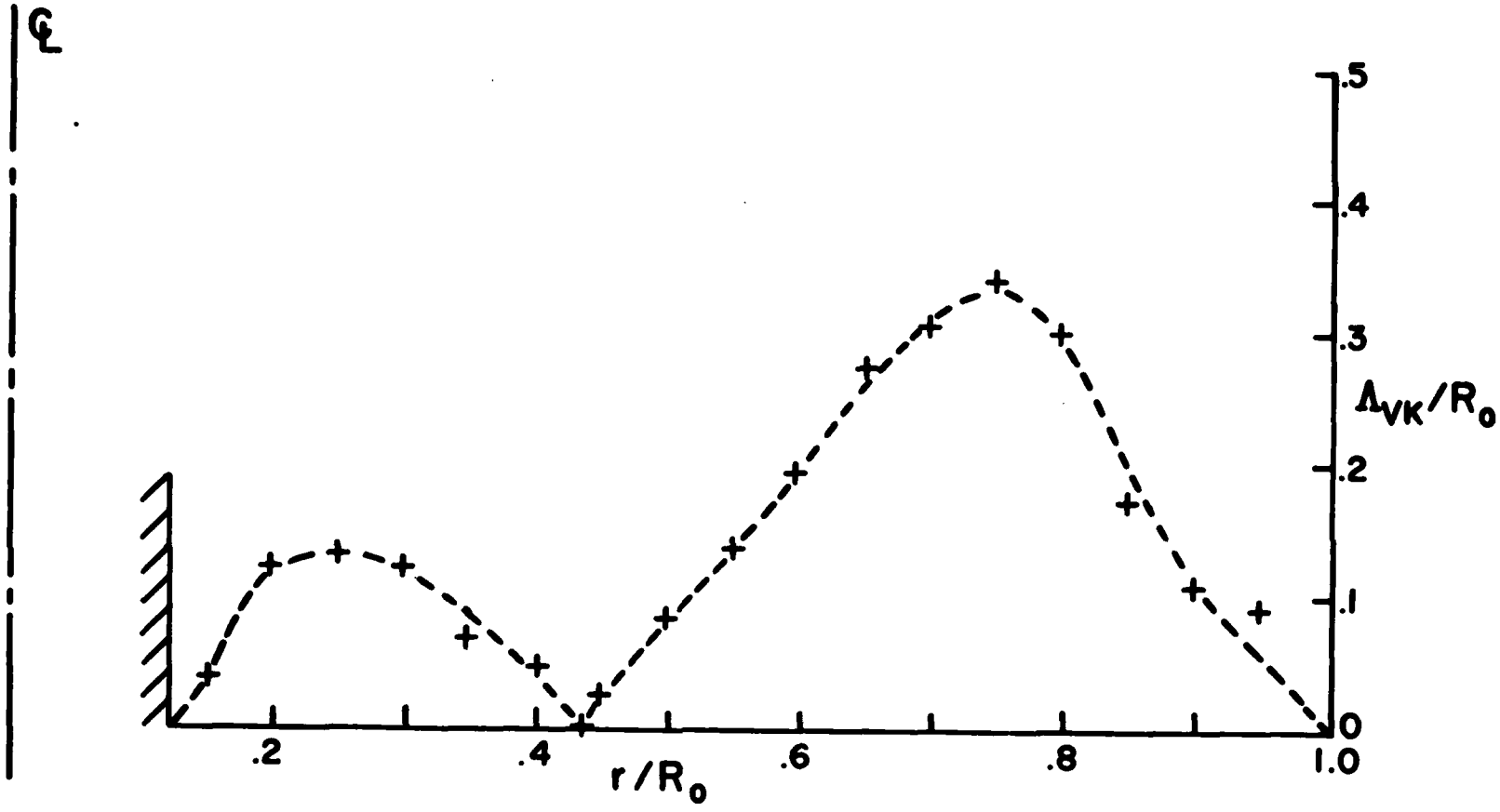

Figure 11 - The von Karman length scale vs. radial position for the present experimental data.

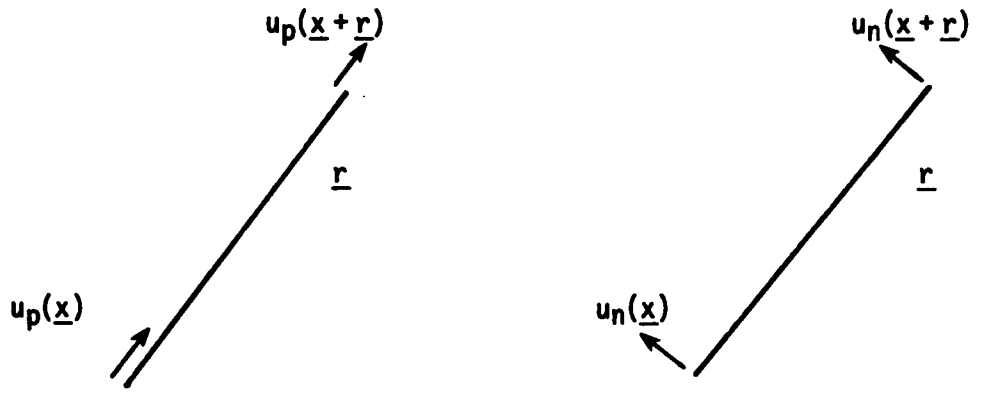

$$u_p(\underline{x})\, u_p(\underline{x}+\underline{r}) = u^2 f(r)$$

$$u_n(\underline{x})\, u_n(\underline{x}+\underline{r}) = u^2 g(r)$$

$$u_p^2 = u_n^2 = u^2$$

Figure 12 - Schematic of perpendicular and normal velocities and their orientations to the separation vector, $\underline{r}$.

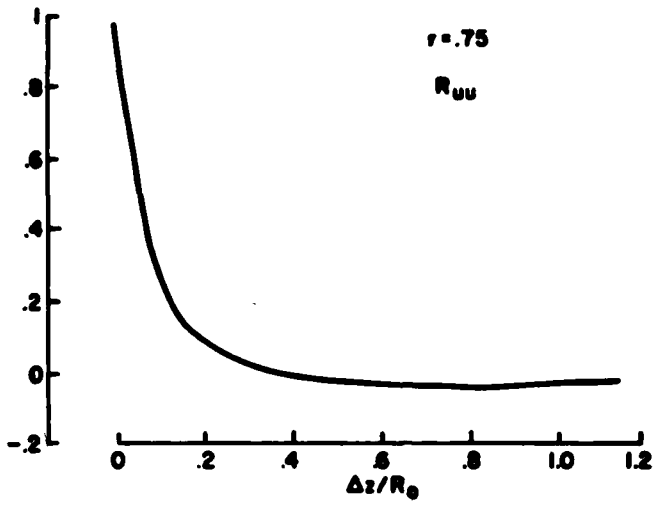

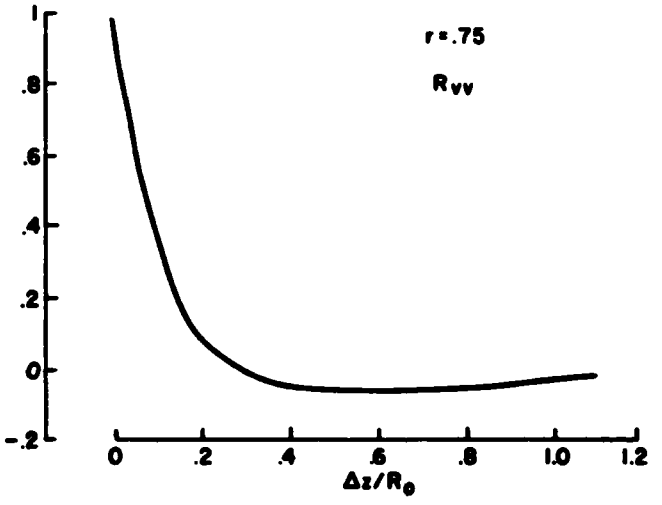

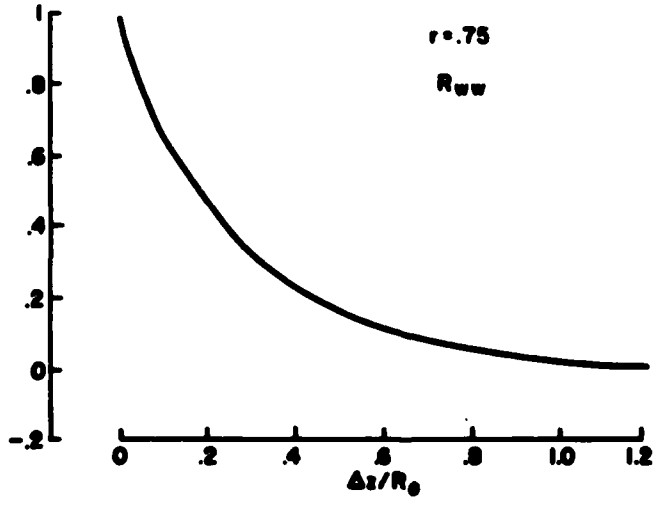

Figure 13 - Correlations for the three velocity components as a function of axial separation.

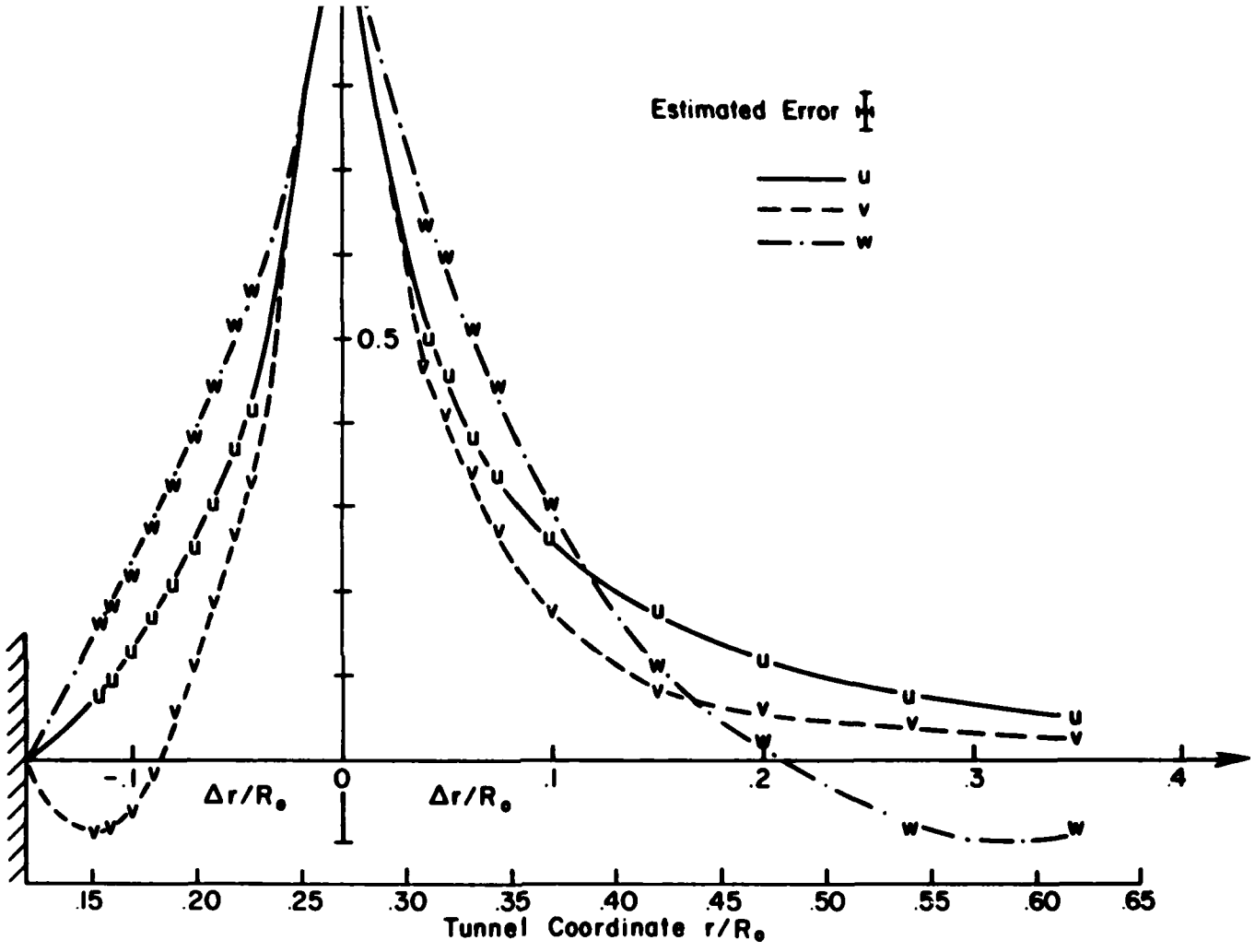

Figure 14 - Correlation for the velocity components as a function of radial separation; $r_F = .27$.

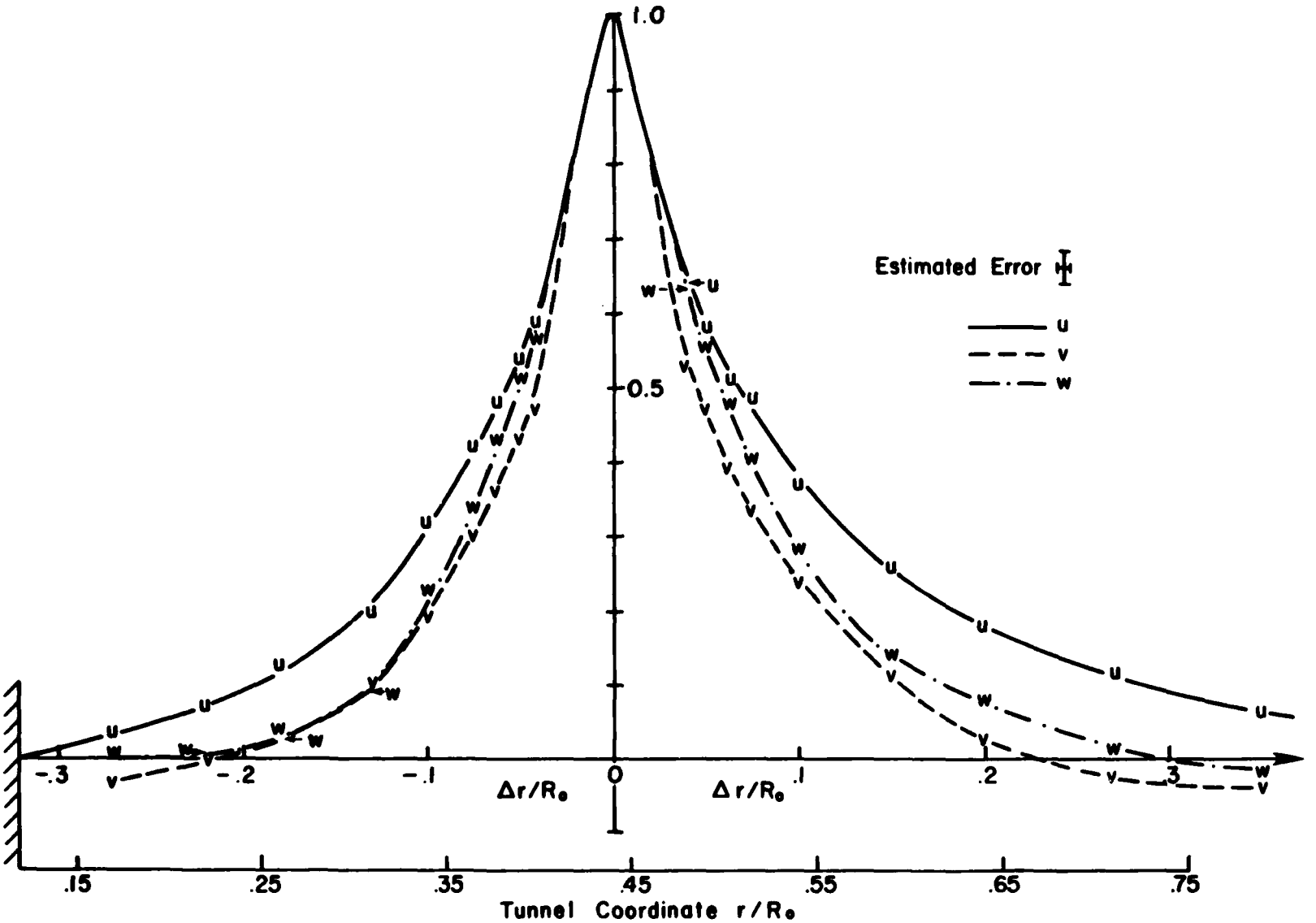

Figure 15 - Correlation for the velocity components as a function of radial separation; $r_F = .43$.

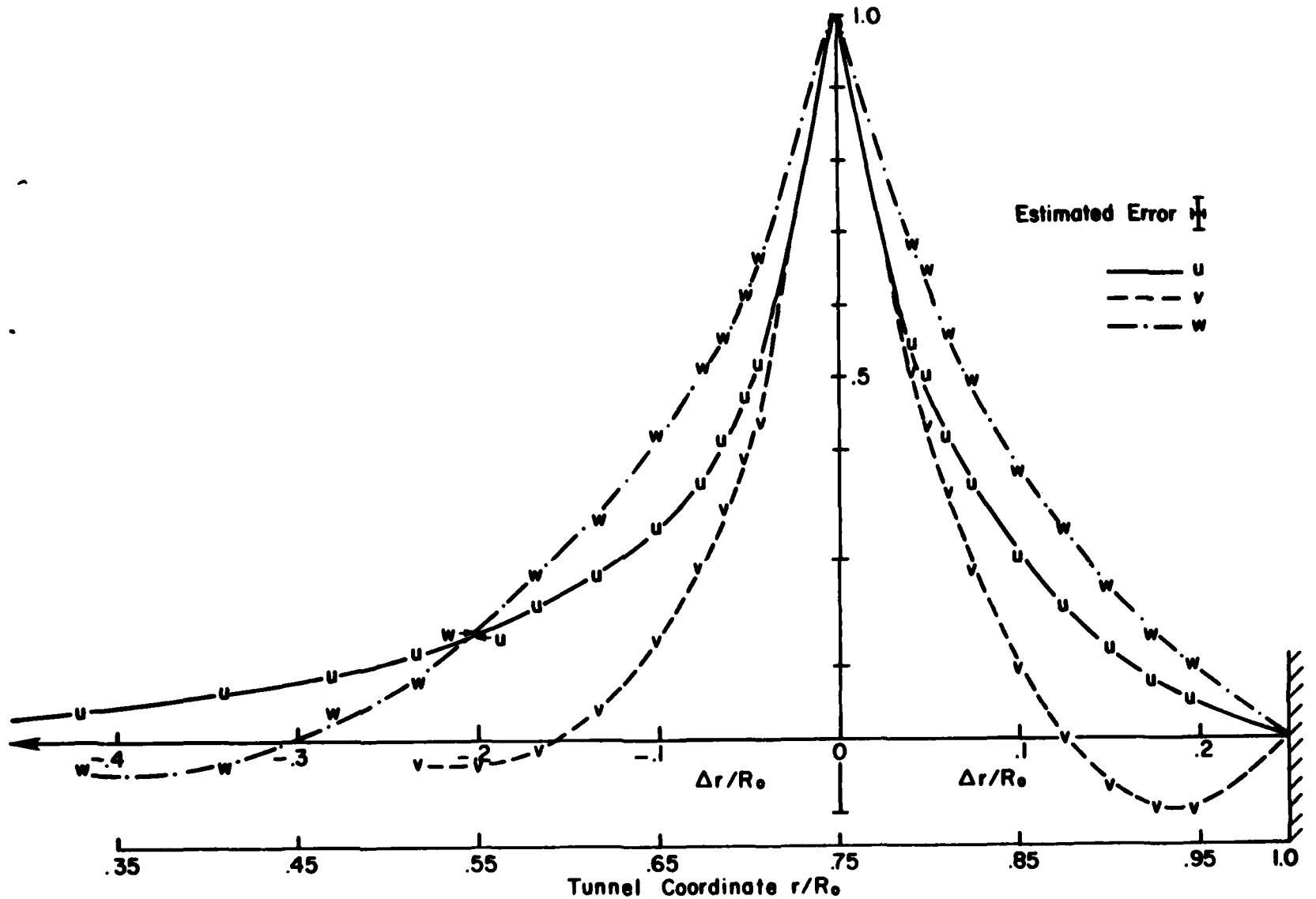

Figure 16 - Correlation for the velocity components as a function of radial separation; $r_F = .75$.

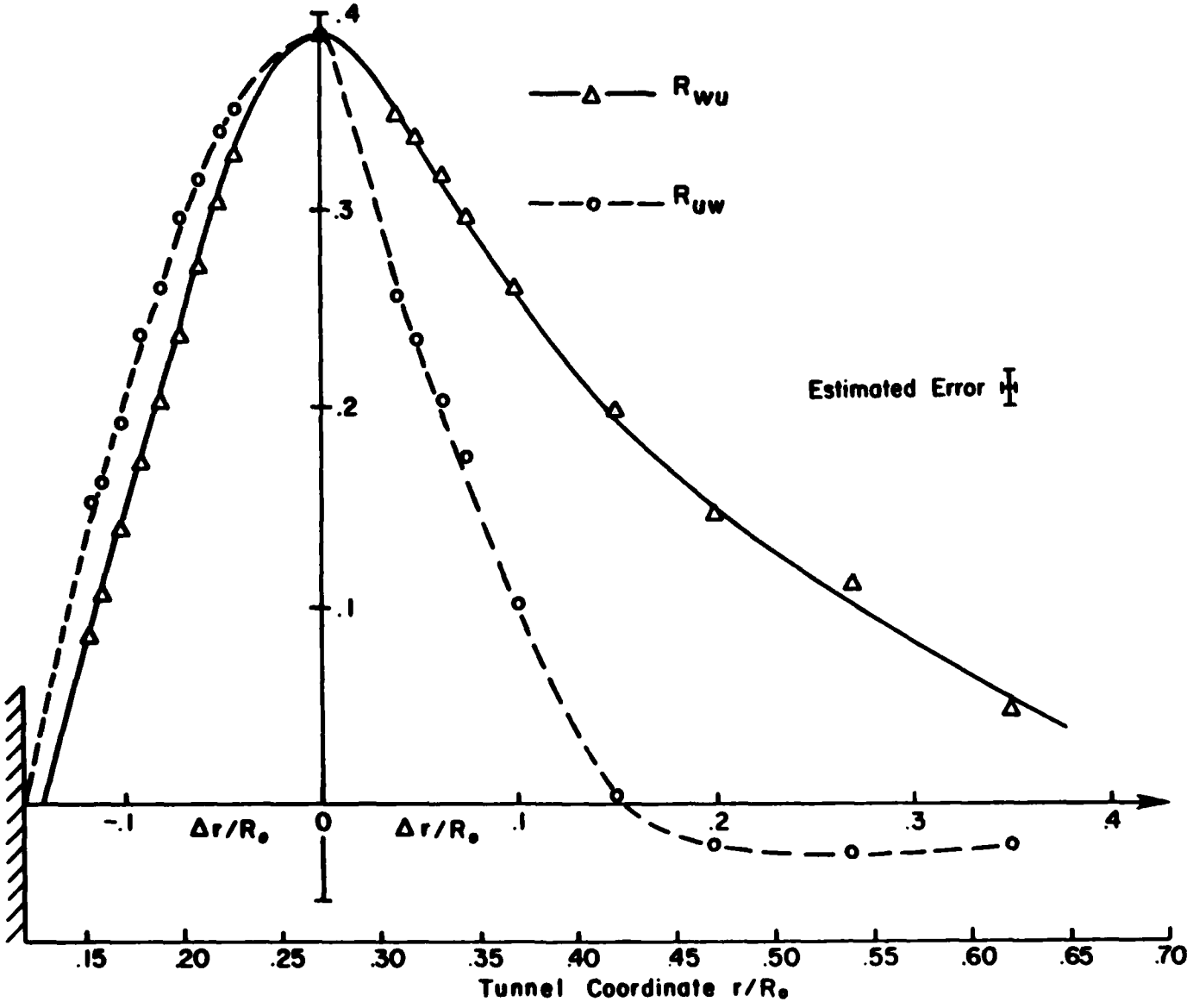

Figure 17 - Cross-correlations for u and w as a function of radial separation; $r_F = .27$.

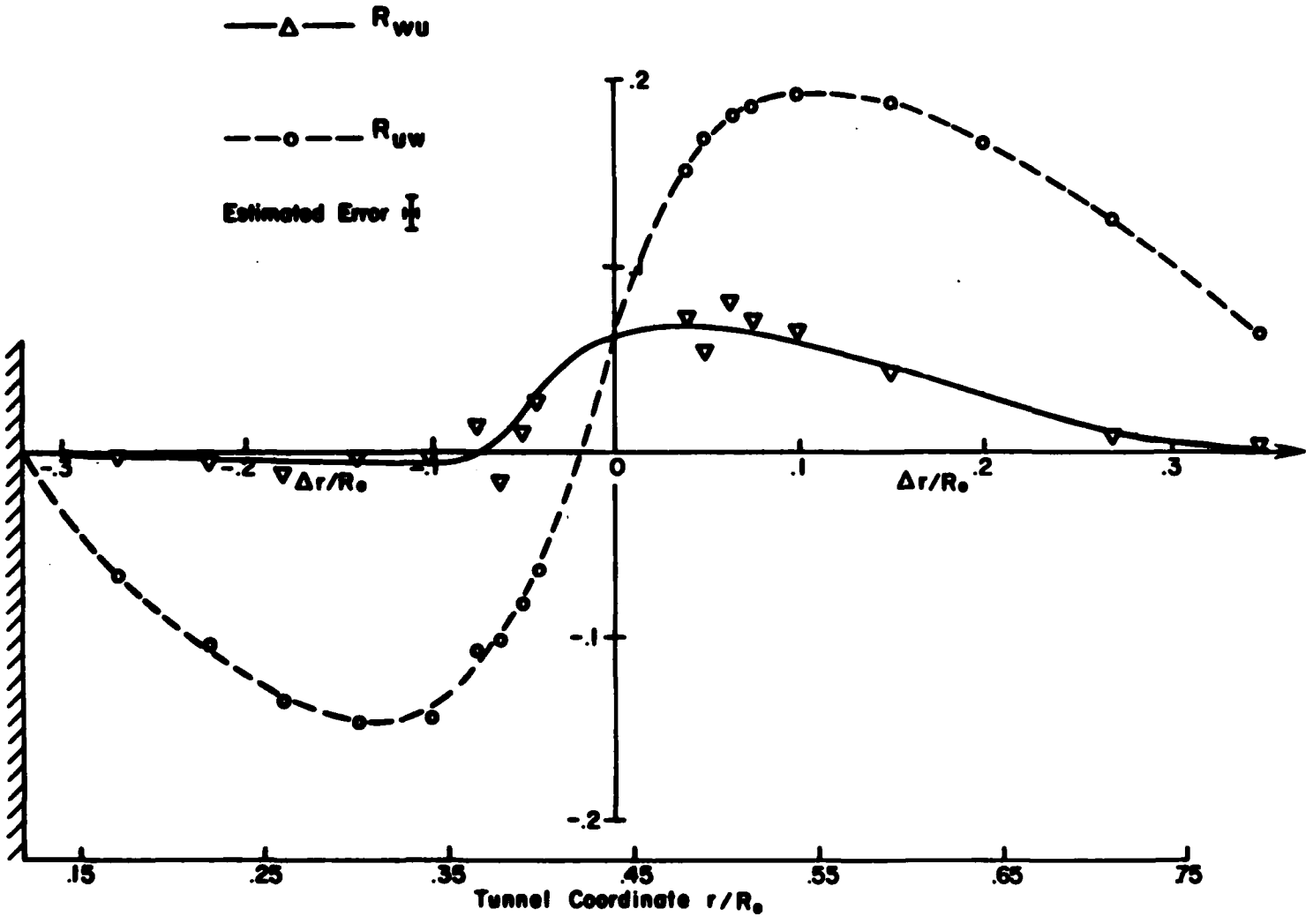

Figure 18 - Cross-correlations for u and w as a function of radial separation; $r_F = .43$.

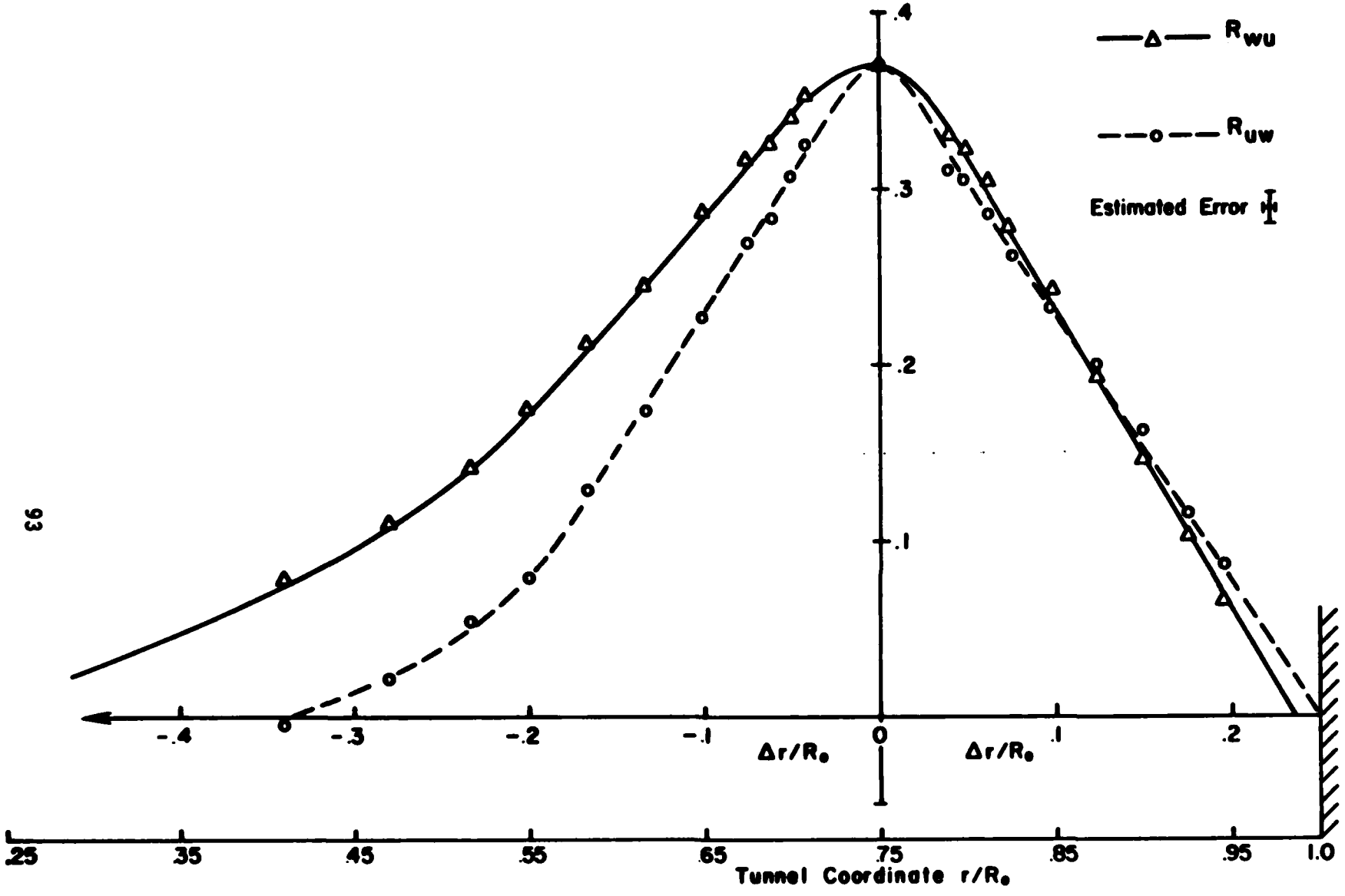

Figure 19 - Cross-correlations for u and w as a function of radial separation; r_F = .75.

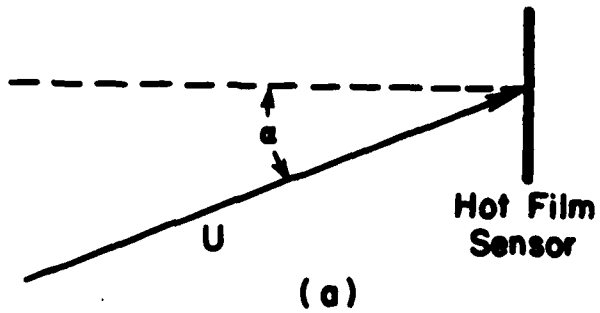

(a)

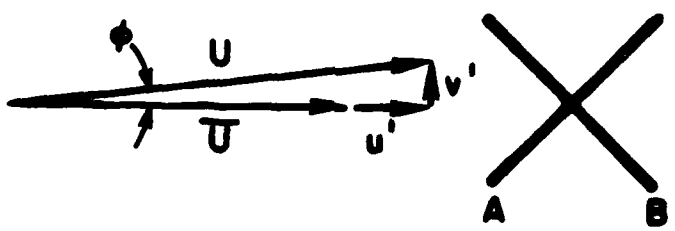

(b)

Figure A1 - Orientations of the mean and instantaneous velocities to hot filter sensors.


N
DAT